








RESEARCH ARTICLE | JULY 09 2024

Multiple boundary layer suction slots technique for performance improvement of vertical-axis wind turbines: Conceptual design and parametric analysis

Special Collection: [Flow and Civil Structures](#)

Rui Zhang (张睿) ; Limin Kuang (况利民) ; Yu Tu (涂瑜); Zhikun Dong (董之坤); Huan Ping (平焕); Kai Zhang (张凯) ; Zhaolong Han (韩兆龙) ; Dai Zhou (周岱)  ; Yan Bao (包艳) 



Physics of Fluids 36, 075126 (2024)

<https://doi.org/10.1063/5.0214013>



Articles You May Be Interested In

Novel passive flow control method using leading-edge prism-shaped cylinder: Performance enhancement of vertical-axis wind turbines

Physics of Fluids (November 2024)

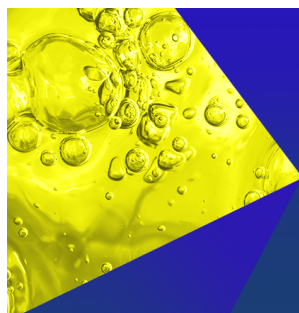
A systematic study on the aerodynamic performance enhancement in H-type Darrieus vertical axis wind turbines using vortex cavity layouts and deflectors

Physics of Fluids (December 2024)

Study on approach of performance improvement of VAWT employing double multiple stream tubes model

J. Renewable Sustainable Energy (March 2017)

28 November 2025 04:17:12



Physics of Fluids
Special Topics
Open for Submissions

[Learn More](#)

Multiple boundary layer suction slots technique for performance improvement of vertical-axis wind turbines: Conceptual design and parametric analysis

Cite as: Phys. Fluids **36**, 075126 (2024); doi: [10.1063/5.0214013](https://doi.org/10.1063/5.0214013)

Submitted: 15 April 2024 · Accepted: 18 June 2024 ·

Published Online: 9 July 2024



Rui Zhang (张睿),¹ Limin Kuang (况利民),¹ Yu Tu (涂瑜),^{1,2} Zhikun Dong (董之坤),³ Huan Ping (平焕),⁴ Kai Zhang (张凯),¹ Zhaolong Han (韩兆龙),^{1,5} Dai Zhou (周岱),^{1,6,a)} and Yan Bao (包艳)¹

AFFILIATIONS

¹State Key Laboratory of Ocean Engineering, School of Ocean and Civil Engineering, Shanghai Jiao Tong University, Shanghai 200240, China

²Renewable Energy Research Group (RERG), Department of Building Environment and Energy Engineering, The Hong Kong Polytechnic University, Hong Kong 100872, China

³Department of Civil Engineering, The University of Hong Kong, Pokfulam, Hong Kong 999077, China

⁴College of Ocean Science and Engineering, Shanghai Maritime University, Shanghai 201306, China

⁵Institute of Polar and Ocean Technology, Institute of Marine Equipment, Shanghai Jiao Tong University, Shanghai 200240, China

⁶Shenzhen Research Institute of Shanghai Jiao Tong University, Shenzhen 518063, China

Note: This paper is part of the special topic, Flow and Civil Structures.

^{a)} Author to whom correspondence should be addressed: zhoudai@sjtu.edu.cn

ABSTRACT

Vertical-axis wind turbines (VAWTs) are gaining attention for urban and offshore applications. However, their development is hindered by suboptimal power performance, primarily attributable to the complex aerodynamic characteristics of the blades. Flow control techniques are expected to regulate the flow on the blade surface and improve blade aerodynamics. In the present study, an effective active flow control technique, multiple boundary layer suction slots (MBLSS), is designed for VAWTs performance improvement. The impact of MBLSS on the aerodynamic performance of VAWTs is examined using high-fidelity computational fluid dynamics simulations. The response surface methodology is employed to identify the relatively optimal configuration of MBLSS. Three key parameters are considered, i.e., number of slots (n), distance between slots (d), and slot length (l), which vary from 2 to 4, 0.025c to 0.125c, and 0.025c to 0.075c, respectively. The results show that MBLSS positively affects the power performance and aerodynamics of VAWTs. Parameter n has the most significant effect on VAWT power performance and the importance of d and l is determined by tip speed ratios (TSRs). Tight and loose slot arrangements are recommended for high and low TSRs, respectively. The relatively optimal configuration ($n = 2$, $d = 0.025c$, $l = 0.05c$) results in a remarkable 31.02% increase in the average net power output of the studied TSRs. The flow control mechanism of MBLSS for VAWT blade boundary layer flow has also been further complemented. MBLSS can prevent the bursting of laminar separation bubbles and avoid the formation of dynamic stall vortices. This increases the blade lift-to-drag ratio and mitigates aerodynamic load fluctuations. The wake profiles of VAWTs with MBLSS are also investigated. This study would add value to the application of active flow control techniques for VAWTs.

Published under an exclusive license by AIP Publishing. <https://doi.org/10.1063/5.0214013>

I. INTRODUCTION

Owing to the consuming of fossil fuels, the energy markets are constricted, which has impelled governments to apportion augmented financial resources toward the advancement of renewable energy, including wind energy.¹ As the most common wind energy conversion

device, wind turbines can be categorized into horizontal-axis wind turbines (HAWTs) and vertical-axis wind turbines (VAWTs).² In recent years, VAWTs have gained attention for their ability to harness wind from all directions, the economical maintenance of gearboxes, and the simplicity of manufacturing blades.³

TABLE I. Geometrical parameters of the VAWT.

Parameter	Value
Airfoil profile	NACA0018
Blade number (N)	2
Blade chord length (c)	0.06 m
Rotor diameter (D)	1 m
Blade span length (h)	1 m
Solidity (Nc/D)	0.12
Blade aspect ratio (h/c)	16.67

However, complex aerodynamic characteristics at low tip speed ratios (TSRs) impede the application and development of VAWTs, attracting the attention of scholars for the improvement of VAWT aerodynamics. The VAWTs blade flow phenomena such as dynamic stall and the vortex shedding are driven by the geometrical and operational characteristics of the turbine, but also can be improved by blade flow control, which can regulate boundary layer behavior and suppress flow separation and dynamic stall. Depending on whether additional energy input is required, flow control techniques can be categorized as passive and active. Passive flow control techniques mainly include slots,^{4,5} dimples,⁶ vortex generators,^{7,8} Gurney flaps (GF),^{9–11} and leading-edge microcylinders.¹² However, the effectiveness of passive flow control techniques is not good enough and may be limited at high TSRs. Mohamed *et al.*⁵ generated a y-direction slot at the leading edge (LE) of VAWT blade. The results show that although the slotted airfoil effectively delay the boundary layer separation at low TSR, the blade power generation will be worse at high TSRs. Bianchini *et al.*¹⁰ mounted GF at the trailing edge (TE) of the VAWT airfoil and found GF could improve the VAWT power generation by 21.3% at low TSR. However, as TSR increases, the power generation returns will gradually diminish. Given that VAWTs are often deployed in urban areas characterized by

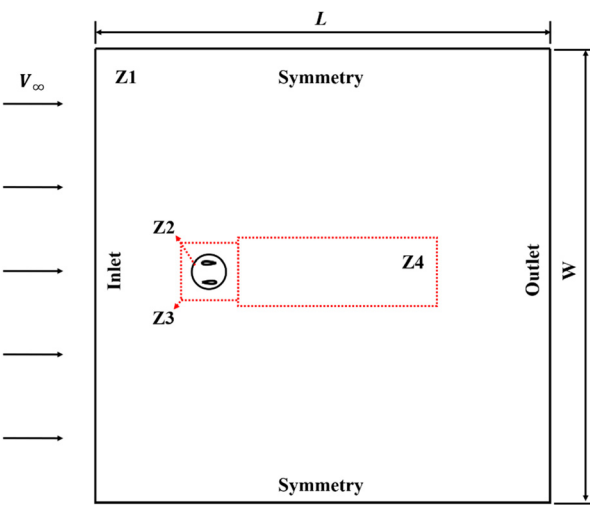


FIG. 2. Plan view of the computational domain.

TABLE II. Average C_p of the reference VAWT for different mesh topologies (TSR = 2.5).

Mesh topology	C_p	Grid count	ΔC_p	Maximum y^+ on blades
Very coarse	0.044 78	287 275	−3.720	1.4929
Coarse	0.044 77	340 000	−3.741	1.4851
Middle	0.045 12	423 038	−2.989	1.4839
Fine	0.046 25	551 154	−0.559	1.5053
Very fine	0.046 51	731 221	...	1.5194

turbulent and variable-direction low-speed wind conditions,¹³ which typically correspond to high TSRs when the VAWT rotation speed is fixed, the utility of passive control techniques may be somewhat limited.

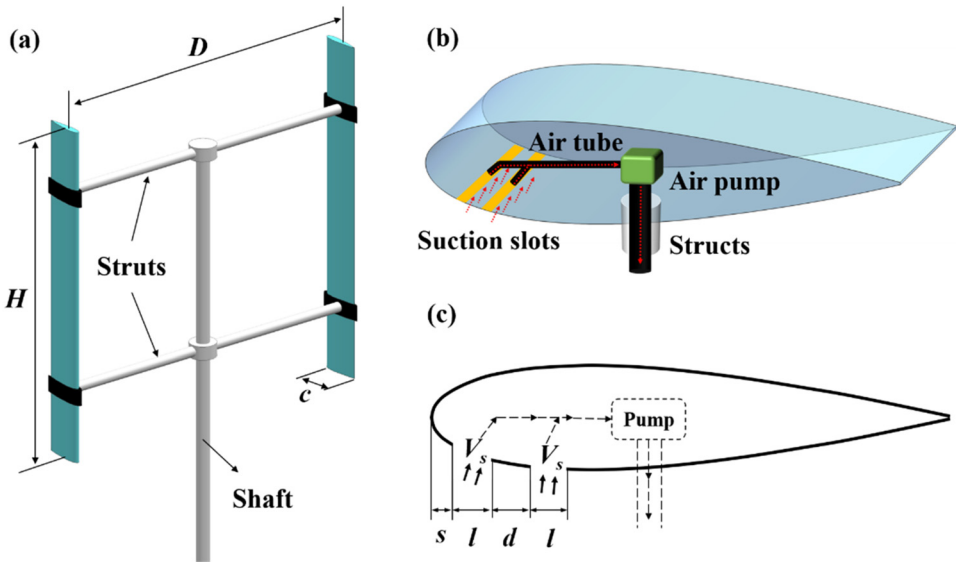


FIG. 1. Conceptual design of MBLSS applied to the VAWT: (a) Overview; (b) plan view of MBLSS; and (c) geometrical specifications of MBLSS.

TABLE III. Boundary layer meshing strategy of MBLSS.

Wall region	First grid height (mm)	Growth ratio	Grid layer number	Total thickness (mm)	Minimum surface grid size (mm)
Blade wall	6.601×10^{-3}	1.1	27	0.8	0.15
Slots refine	6.622×10^{-3}	1.05	40	0.8	0.02
Suction slots	6.629×10^{-3}	1.02	62	0.8	0.02

From this perspective, the active flow control technique holds immense potential in achieving substantial power gains, making it invaluable for the development of VAWTs. A number of active flow control techniques have been proposed, including plasma actuators,^{14,15} synthetic jets,¹⁶ moving surfaces,^{17,18} boundary layer suction/blowing,^{19,20} pitch control,²¹ and oscillating TE flaps.²² Among these, boundary layer suction is an important approach to extracting fluid from ambient flow and has proven to be effective in regulating the flow on the blade surface. Moussavi *et al.*²³ proposed and investigated the boundary layer suction technique on a megawatt (MW) class wind

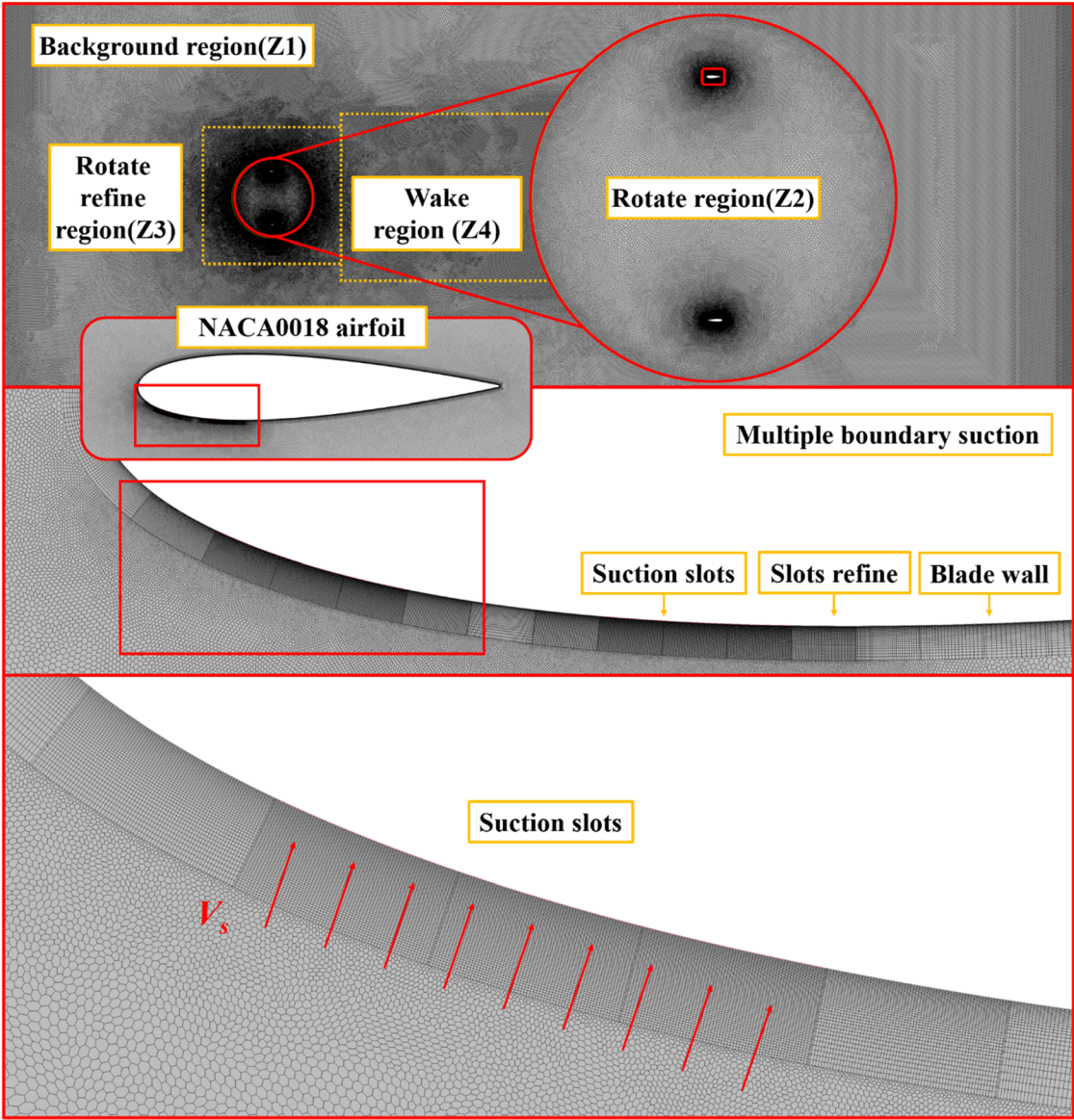


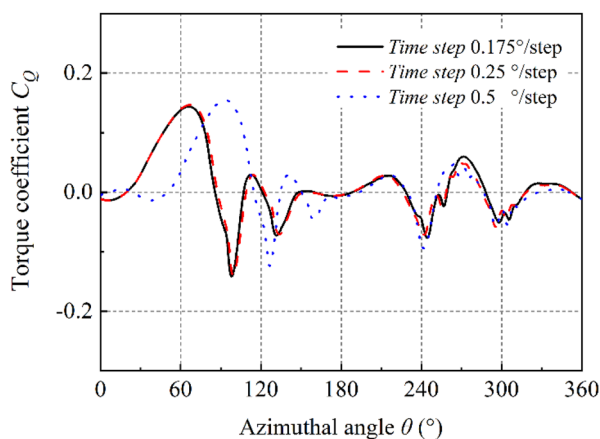
FIG. 3. Mesh topology of the computational domain.

TABLE IV. Parameters for the single suction slot and the micropump.

Parameter	Value
Single suction slot	
Slot length	0.0015 m (0.025c)
Suction velocity	0.0465 m/s
Volume flow rate per blade with unit span	4.185 l/min
Micropump	
Flow rate	5 l/min
Vacuum depth	deeper than 80 kPa
Voltage	12 V
Power consumption	4–6 W

turbine. Their study demonstrates that by implementing a narrow slot at the inboard section of the blade, the power coefficient (C_p) of the rotor can be enhanced by up to 8.1%. Aldabash *et al.*²⁴ applied blowing/suction techniques to the NREL S822 profile and found that it enhances the wind turbine performance by an average of 15%. You *et al.*¹⁶ performed suction technique for an airfoil by computational fluid dynamics (CFD) simulations. The results show that the suction extracts the low momentum boundary layer flow in the suction phase, preventing downstream flow separation. FatahiAn *et al.*²⁵ carried out a CFD investigation for an cavity airfoil equipped with a suction slot and found that suction slot will enhance the blade lift-to-drag rate obviously, which is beneficial for straight blade VAWTs. Rezaeiha *et al.*²⁶ installed the boundary layer suction slot (BLSS) on VAWTs. The CFD results show that the performance enhancement of the wind turbine due to suction is insensitive to the change of suction velocity and the average power output of the wind turbine is maximized when the position of the suction slot is located at the LE of blade.

The effective control of the boundary layer by the suction slot is well documented. The control mechanism is mainly through the extraction of low-energy fluid to destroy the boundary layer. Then the outer high-energy fluid is forced to flow in to achieve the reformation of the boundary layer, so as to make the wall flow more attached. However, a single suction slot has a limited influence area and does not provide good control of the entire boundary layer. Adopting a multiple suction

**FIG. 4.** Instantaneous torque coefficients of the blades during one turbine revolution for different time step topologies (TSR = 2.5).**TABLE V.** RSM orthogonal results.

No.	n	d	l	TSR = 2.5	TSR = 3.25	TSR = 4
				C_{p-net}	C_{p-net}	C_{p-net}
0 (Baseline)	0.0428	0.3096	0.4269
1	3	0.075c	0.050c	0.1818	0.3792	0.4316
2	4	0.025c	0.050c	0.1598	0.3638	0.4368
3	3	0.025c	0.025c	0.1936	0.4130	0.4758
4	3	0.025c	0.075c	0.1473	0.3566	0.4430
5	2	0.075c	0.025c	0.1980	0.4170	0.4656
6	2	0.125c	0.050c	0.2221	0.4204	0.4776
7	3	0.125c	0.025c	0.1964	0.3988	0.4301
8	4	0.125c	0.050c	0.1098	0.2829	0.3214
9	3	0.075c	0.050c	0.1818	0.3792	0.4316
10	4	0.075c	0.025c	0.1863	0.3854	0.4187
11	3	0.075c	0.050c	0.1818	0.3792	0.4316
12	3	0.075c	0.050c	0.1818	0.3792	0.4316
13	3	0.125c	0.075c	0.0917	0.2820	0.3406
14	4	0.075c	0.075c	0.0290	0.2147	0.2715
15	3	0.075c	0.050c	0.1818	0.3792	0.4316
16	2	0.075c	0.075c	0.1995	0.4042	0.4748
17	2	0.025c	0.050c	0.1989	0.4181	0.5063

strategy can extend the influence range of suction control and further improve the blade performance. Ohashi *et al.*²⁷ installed two blowing and two suction blades on a static Clark-Y wing and found that the lift coefficient of the blades increased by 10%. Elsayed *et al.*²⁸ installed multi-suction jets on static NACA0012 airfoil and carry out experiments and numerical simulations to investigate the aerodynamic characteristics. They pointed out that the effect of multi-suction jets overrides single suction jet and can make the wall flow stable and eventually remains a laminar boundary layer. Sun *et al.*²⁹ set up multiple boundary layer suction slots (MBLSS) on static airfoil blades and extensively investigated their effects on flow fields surrounding the blades. The findings reveal that, under a constant suction momentum, multiple suction slots can further improve the performance of airfoils and VAWT compared to single suction slot. Previous studies have demonstrated that the impact of MBLSS on the flow field around static blades surpasses that of BLSS. MBLSS is expected to yield more effective flow control, suppressing flow separation and dynamic stall on the blade surface, thereby improving the overall performance of VAWTs. However, despite its evident potential, the application of MBLSS in VAWTs remains largely unexplored, necessitating further investigation and research in this domain.

Therefore, this study is dedicated to

- Examine the impact of MBLSS on the power performance of VAWTs using high-fidelity CFD simulations.
- Characterize the geometrical effect of MBLSS and determine the relatively optimal configuration based on response surface methodology (RSM).
- Analyze the aerodynamic loads and flow patterns of the blades to explore the flow control mechanism of MBLSS.

To our knowledge, this study is the first to design and examine the effectiveness of MBLSS for VAWTs, thus introducing a novel

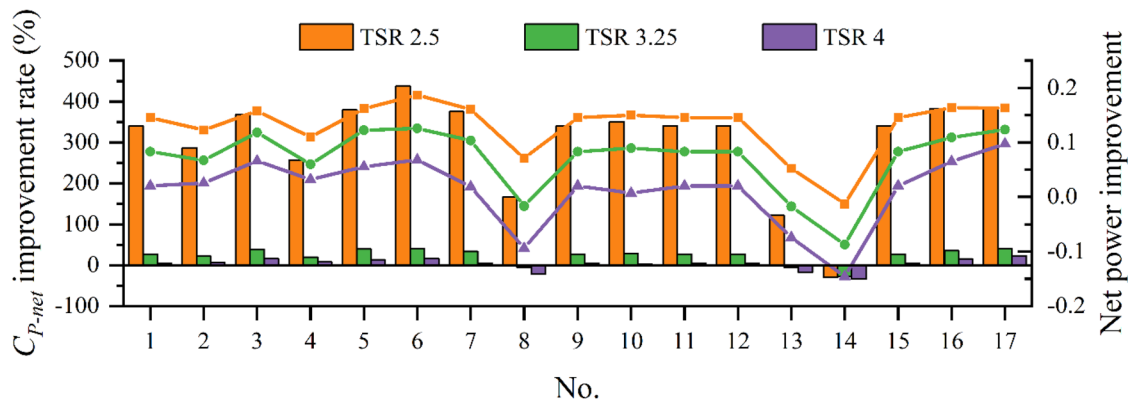


FIG. 5. C_{p-net} improvement rate and power improvement for orthogonal cases.

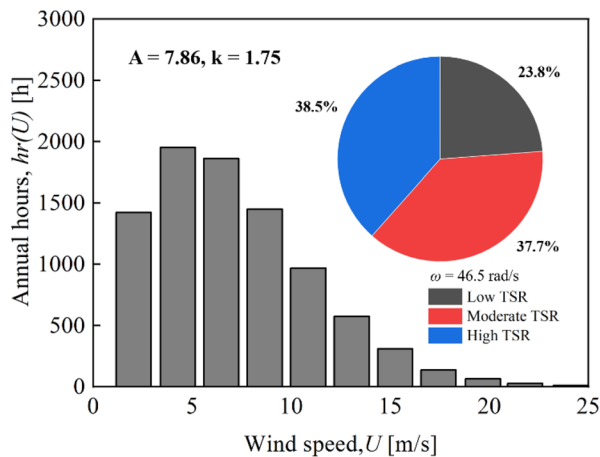


FIG. 6. A test set of annual distribution of hours per wind speed and the corresponding TSR rates.

contribution to the field. The key contributions include (1) the feasibility of applying MBLSS to VAWTs to improve power performance is demonstrated; (2) the importance of the key parameters of MBLSS is clarified and the relatively optimal working conditions are obtained; and (3) the knowledge of how MBLSS suppress flow separation and dynamic stall is enriched.

This paper is structured as follows: Sec. II details the properties of the turbine model, MBLSS system, and numerical model. Section III presents the results and discussion regarding the impact of MBLSS on the power performance and aerodynamics of VAWTs. Section IV provides the concluding remarks.

II. NUMERICAL METHOD

A. Turbine model

In this study, a two-bladed VAWT designed by Tescione *et al.*³⁰ is adopted. The sophisticated design makes the selected VAWT a benchmark that has been widely used in previous validation and optimization studies.^{31,32} The geometrical parameters of the VAWT are shown in Table I.

TABLE VI. The results of ANOVA of all TSRs.

Source	TSR = 2.5		TSR = 3.25		TSR = 4	
	F Value	p-value	F Value	p-value	F Value	p-value
Model	128.57	<0.0001	278.97	<0.0001	397.92	<0.0001
A- <i>n</i>	430.28	<0.0001	1051.28	<0.0001	1740.01	<0.0001
B- <i>d</i>	26.49	0.0013	184.30	<0.0001	693.21	<0.0001
C- <i>l</i>	344.50	<0.0001	746.59	<0.0001	469.62	<0.0001
AB	44.82	0.0003	90.77	<0.0001	121.99	0.0013
AC	202.74	<0.0001	314.59	<0.0001	381.36	<0.0001
BC	28.72	0.0011	47.94	0.0001	52.24	0.0005
A ²	6.16	0.0421	12.74	0.0070	7.87	0.0174
B ²	0.95	0.3618	0.025	0.8160	23.90	0.0153
C ²	68.55	<0.0001	58.86	<0.0001	94.13	0.0063

The conceptual design of MBLSS applied to the VAWT is shown in Fig. 1. Air is drawn in from the suction slots located near the blade LE and exhausted from the top of the shaft. A micropump is used as a power source to deliver air through the air tube. The design of MBLSS is determined by several geometrical parameters, i.e., distance from the first slot to the blade LE (*s*), number of slots (*n*), distance between slots (*d*), and slot length (*l*). The suction velocity (*V_s*) is perpendicular to the blade wall and uniformly distributed along the slot. The micropumps and air tubes are omitted to simplify the numerical modeling. The shaft and struts are also neglected because of their small impact on VAWT aerodynamics.^{33,34} The validation of suction slot technique is presented in supplementary material S1.

TABLE VII. The convincing well results of the regression model.

Parameter	TSR = 2.5	TSR = 3.25	TSR = 4
R^2	0.9940	0.9972	0.9980
R^2_{Adj}	0.9863	0.9936	0.9955
R^2_{Pre}	0.9038	0.9555	0.9688
Adequate precision	43.596	58.872	75.387

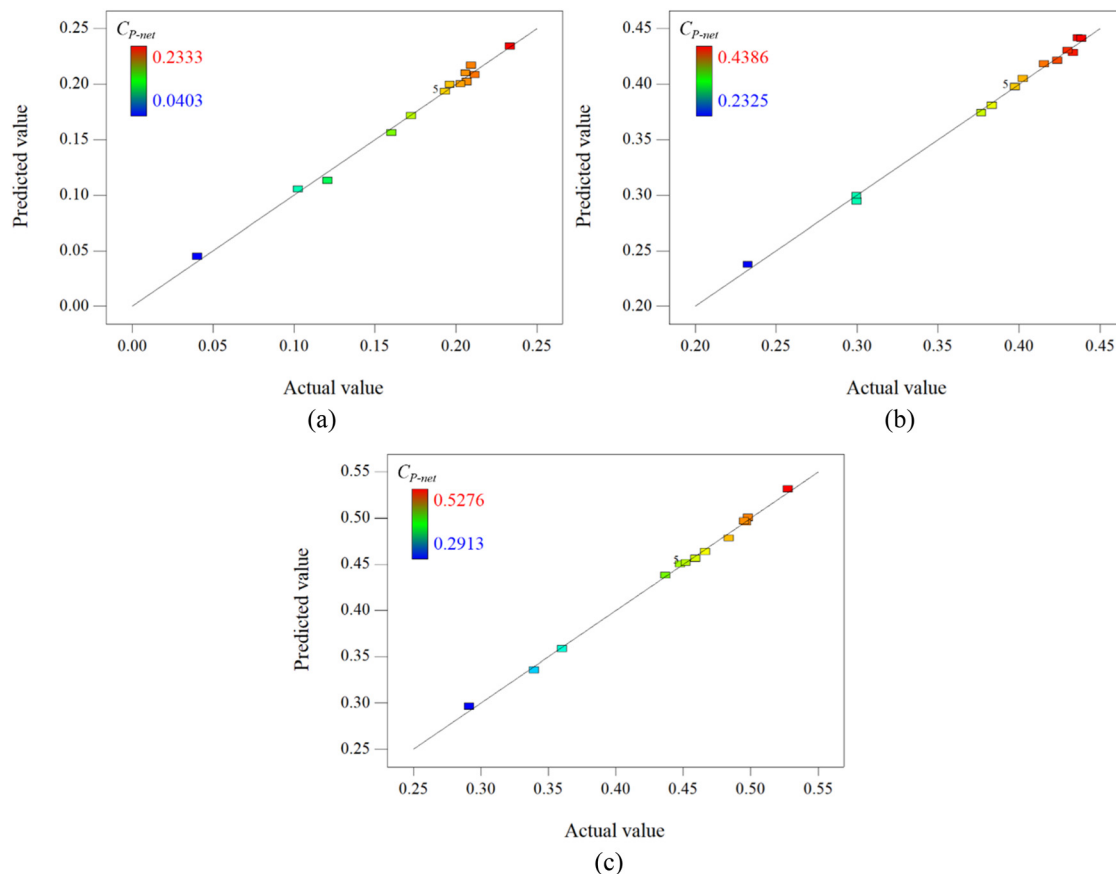


FIG. 7. The comparison of the predicted values and the actual values: (a) TSR = 2.5; (b) TSR = 3.25; and (c) TSR = 4.

B. Computational domain

The two-dimensional (2D) computational domain is shown in Fig. 2. The domain consists of four regions, i.e., background region (Z1), rotating region (Z2), refined region (Z3), and wake region (Z4). The information exchange between Z1 and Z2 is realized using the sliding mesh technique. The dimensions of the domain are set based on the recognized and utilized VAWT guideline.³⁵ The velocity inlet ($V_\infty = 9.3$ m/s) is positioned at a distance of $5D$ from the VAWT,^{36,37} while the pressure outlet is located $25D$ away from it, with a value of 0 Pa. Z2 has a diameter of $1.5D$. The top and bottom sides of the domain are defined as symmetry planes, whereas the VAWT surface is set as a no-slip wall.

The mesh independence of the reference VAWT is shown in Table II. Five mesh topologies are studied and the converged C_p are compared. Note that the aerodynamic parameters of the VAWT are recorded at the 21st turbine revolution, defined as the point where the average values between two consecutive revolutions vary by less than 0.1%. Considering that the complex aerodynamic phenomena occur mainly at low tip speed ratios (TSRs), the TSR = 4.5 applied in the reference wind turbine³⁰ is not utilized here, and instead a lower TSR = 2.5 is adopted. It can be seen that the power difference between the fine and very fine grids is small even when TSR is low. Considering the computational accuracy and computational resources, the fine

mesh is finally selected as the basic meshing strategy in this work. High-resolution quadrilateral grids are distributed around the blades. The VAWT operates within a chord-based Reynolds number range of 1.25×10^5 – 1.75×10^5 . To ensure an accurate examination of the viscous sublayer flow behavior, boundary layer grids are implemented on the blade walls, and the detailed meshing strategy is shown in Table III. The first grid height is determined based on the criterion that the maximum y^+ value remains below 1 throughout the simulations. The mesh topology of the computational domain is illustrated in Fig. 3.

C. Solver setup

The commercial CFD software STAR-CCM+ 13.04.10 is employed for transient simulations. In this study, 2D numerical modeling is adopted for the following reasons: (1) The MBLSS simulation is minimally affected by the 3D tip effect because the blade aspect ratio of the target VAWT is up to 16.77, which exceeds the critical value of 10.³⁸ (2) Extensive precedent exists for the use of 2D numerical modeling in the aerodynamic design and optimization of the same VAWT.^{26,39–41} The validity of 2D CFD simulations has been well documented. Details of the validation of the present numerical model are given in supplementary material S2.

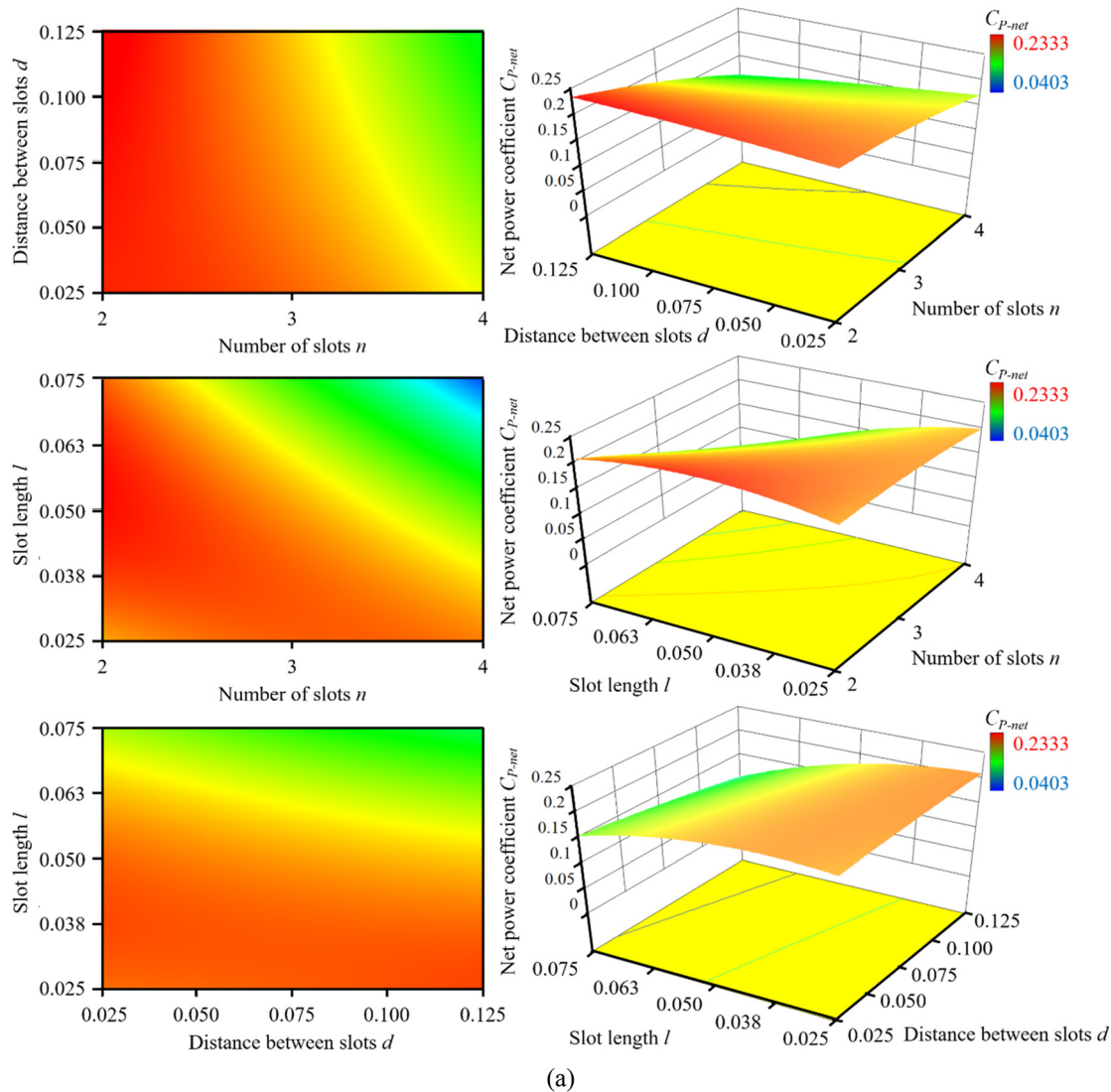


FIG. 8. The cloud plot and the response surface of the effect of the interaction between parameters on C_{p-net} : (a) TSR = 2.5; (b) TSR = 3.25; and (c) TSR = 4.

MBLSS can be considered as a combination of single suction slots. The parameters of a single suction slot are shown in Table IV. For example, for an MBLSS of $n = 2$, $d = 0.075c$, and $l = 0.075c$ (hereafter referred to as $n2d0.075cl0.075c$ for brevity), it can be considered as a combination of two three-single-suction-slot systems. Note that friction losses in the air tubes are not considered in this study.

The unsteady Reynolds-averaged Navier–Stokes (URANS) method is employed for CFD simulations. Considering the complex blade boundary layer behavior, the simulations adopt the γ - Re_θ transition shear stress transport (SST) model.^{42,43} This model is an extension of the two-equation SST k - ω model^{44,45} and incorporates the intermittency γ and the momentum-thickness Reynolds number Re_θ , enabling prediction of the laminar-to-turbulent transition. In terms of

discretization, both the temporal and spatial schemes are set to second order. The pressure–velocity coupling is achieved by the SIMPLE algorithm. The torque coefficient curves of the VAWT under the fine meshing strategy at TSR 2.5 with different time step topologies are shown in Fig. 4. It can be seen that the flow characteristics of the VAWT will not be well presented when the time step is large. Considering the computational accuracy and the computational resources, 0.25° with 20 inner iterations is chosen as the basic computational time step for the present study, which is also a common setting for VAWT CFD simulations.^{46,47}

III. RESULTS AND DISCUSSION

A. Response surface methodology results analysis

Unfortunately, the use of CFD methods for fine-grained computation implies a huge amount of computational effort, and thus it is

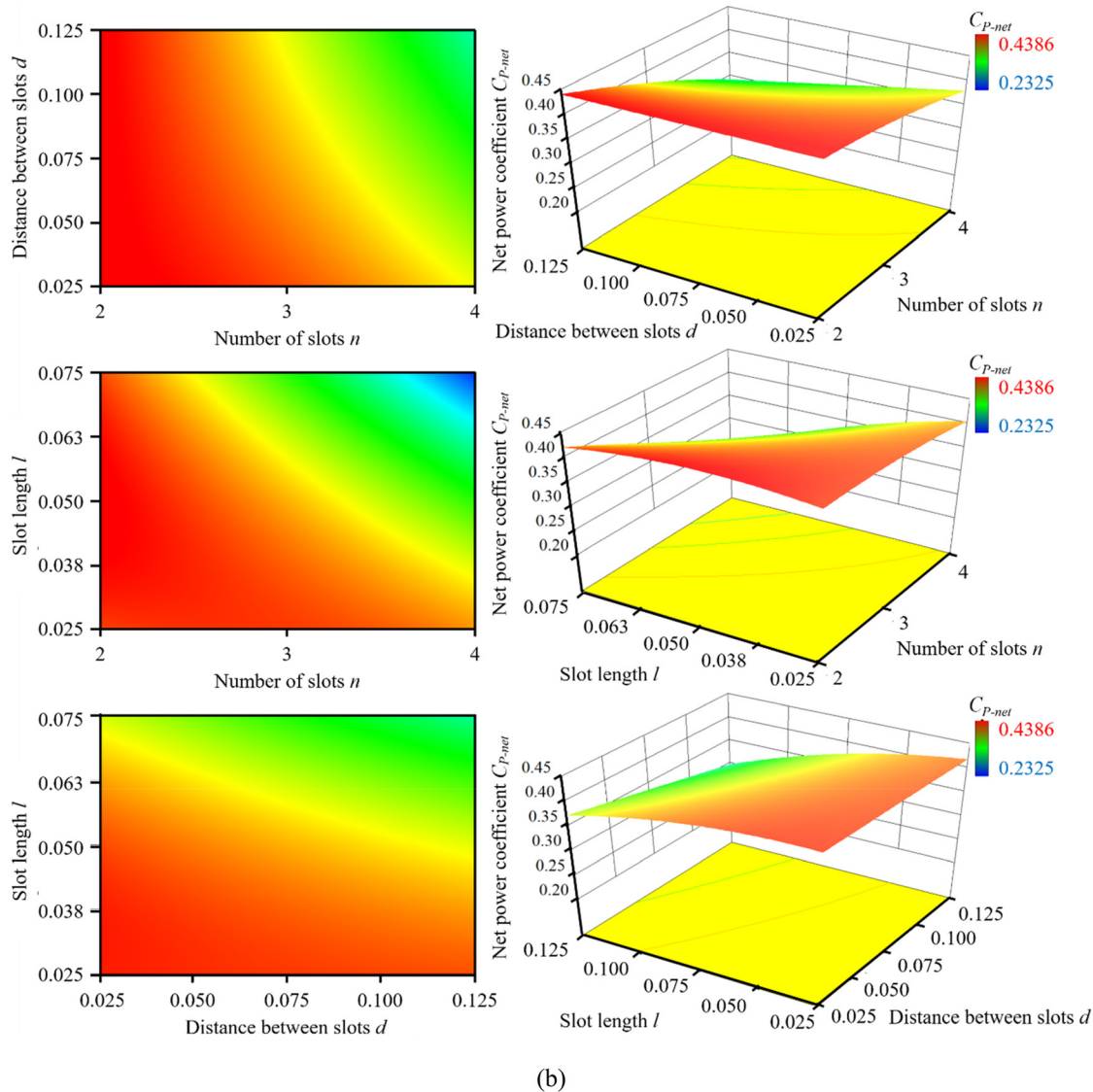


FIG. 8. (Continued).

uneconomical to traverse the arithmetic cases over the linear space consisting of each parameter. The response surface methodology (RSM)⁴⁸ is a typical orthogonal test method, which can reveal the relationship between the multiple factors with multiple levels cases. The main goal of RSM is to find the optimal combination of input variables that maximizes or minimizes the correlated response. This is usually achieved by fitting a response surface, which is a mathematical model that approximates the relationship between the input variables and the response.

1. The Box-Behnken design results

Numerical simulations are conducted following the Box-Behnken design⁴⁹ to assess the performance of VAWTs with MBLSS.

Geometrical parameters are considered within the orthogonal design. Due to the blade surface size limitation, the key geometrical parameters are not fully independent; instead, they adhere to the following relationship equation:

$$s + nl + (n - 1)d \leq c. \quad (1)$$

Unraveling the independent effects of s , n , d , and l on wind turbine performance poses a challenge, making it more meaningful to explore the synergistic relationships among these parameters. According to Rezaeiha's work,²⁶ the first suction slot was suggested to arranged in the LE of blade interface due to the location of flow separation point in the suction side of blade. Therefore, a relatively conservative value of $s = 0.04c$ is utilized. Considering the degree of impact of each parameter on MBLSS and the limitation of blade chord length, a

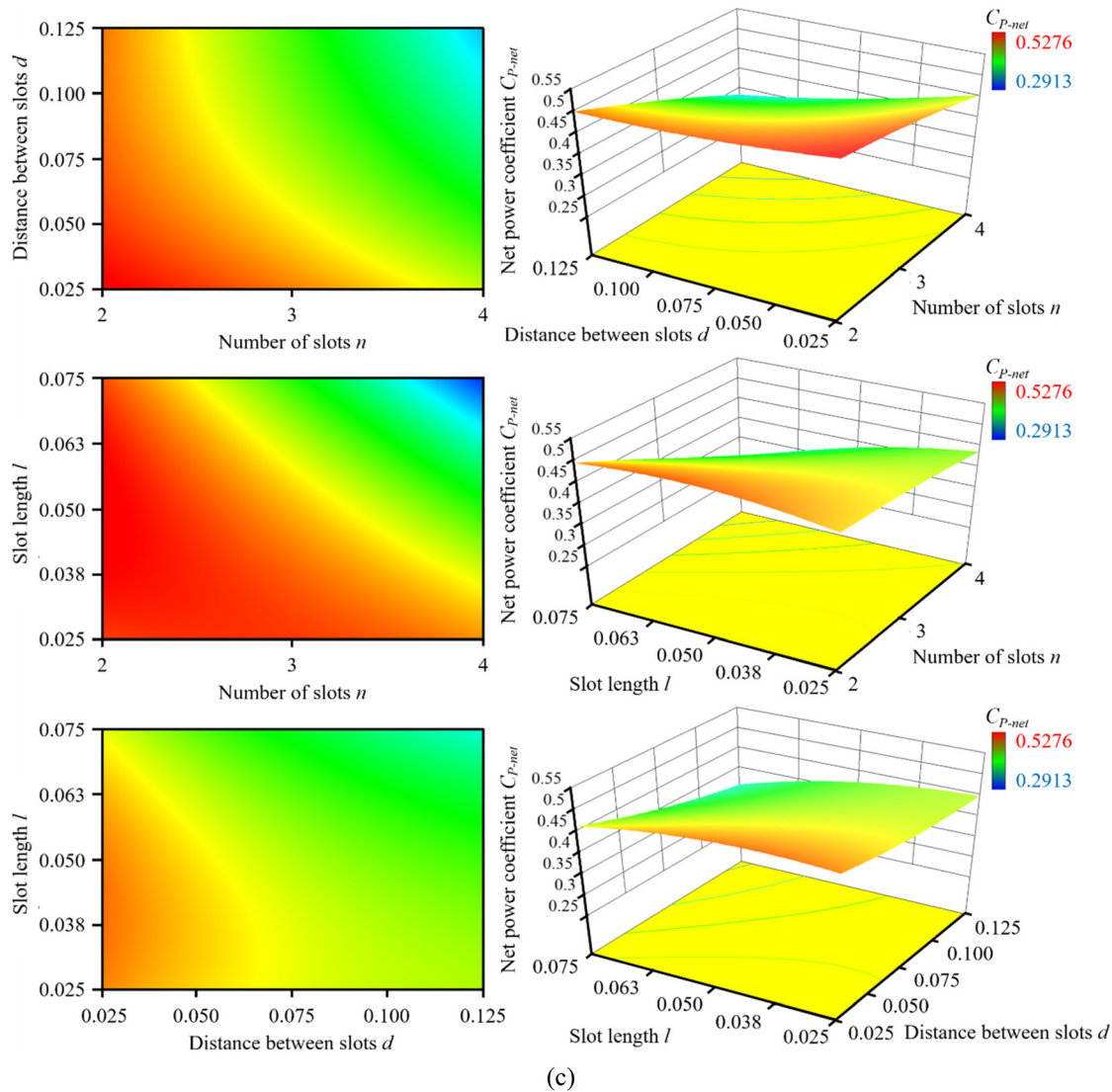


FIG. 8. (Continued).

three factors orthogonal test with three levels are designed and the range of the parameters are 2–4, 0.025–0.125, 0.025–0.075, for n , d , l , respectively. The same design conditions are carried out for three classical operating conditions of TSRs = 2.5, 3.25, and 4, which corresponds to low, moderate, and high rotating speeds, respectively. The orthogonal experimental cases and the results are shown in Table V.

The C_{P-net} presented in Table V is the net power coefficient, which have subtracted the external energy input required for active control of the MBLSS. Noticeable improvements in C_{P-net} values of varying degrees can be observed. When TSR = 2.5, the net power enhancement facilitated by MBLSS is highly evident. The $n2d0.125cl0.05c$ leads to a C_{P-net} improvement of 437%. Such a large power increase is mainly due to the torque cancelation in the symmetric phase after the dynamic stall of the two-bladed VAWT. The further

detailed will be shown in Sec. III B 1. The maximum net power gain of 41% and 23% can be achieved at $n2d0.125cl0.05c$ and $n2d0.025cl0.05c$ for TSR = 3.25 and 4, respectively. The relatively unfavorable case is $n4d0.075cl0.075c$, resulting in a 30%, 28%, and 34% C_{P-net} decrease for low, moderate, and high TSRs, respectively. This decrease is primarily attributed to the high number of suction slots which consuming more power than the improvement achieved by the boundary layer enhancement. Although the MBLSS can contribute to a significant improvement in the C_{P-net} of the VAWTs in most of the operating cases, too many suction slots rather reduce the net power output of the VAWTs.

Furthermore, it is evident that the same suction slot arrangement strategy exhibits a similar trend of performance enhancement at different TSRs, i.e., the ideal suction slots arrangement strategy performs well at all TSRs, while the inferior strategy does not show a good

improvement in VAWT power at all TSRs. The relevant results are shown in Fig. 5. The improvement of MBLSS on the C_{P-net} decreases with the increasing of TSRs, i.e., for TSR = 2.5, 3.25, and 4, the effect of MBLSS on the C_{P-net} is -0.003 to 0.190 , -0.077 to 0.129 and -0.136 to 0.101 , respectively. This is associated with the degree of blade suction side flow separation. For the low TSR where the flow separation is more intense, the C_{P-net} increase by MBLSS is more obvious, while for high TSR where the flow is more attached, the C_{P-net} increase by MBLSS is limited. Such results can be corroborated with the study of Rezaeiha *et al.*²⁶

It is one-sided to evaluate the effect of MBLSS on VAWTs only by the C_{P-net} at a single TSR. Therefore, the annual energy production of VAWTs is also utilized to assess the overall impact of MBLSS on VAWTs. The annual distribution of hours per wind speed [$hr(U)$] which is used to evaluate the annual electricity production can be obtained by fitting wind data with a Weibull distribution function.⁵⁰ Without loss of generality, assume the scale parameter $A = 7.86$ and the shape parameter $k = 1.75$ for the Weibull distribution function.^{51,52} The TSR rates corresponding to the $hr(U)$ can be obtained by assuming that the wind turbine rotational speed is 46.5 rad/s, corresponding to an incoming wind speed of 9.3 m/s and TSR = 2.5. The $hr(U)$ and

the corresponding TSR rates are shown in Fig. 6. Under such a composition of TSR, the relatively optimum working condition is $n2d0.025c0.05c$, the annual energy production is 1203 kWh, and the relatively worse working condition is $n4d0.075c0.075c$, the annual energy production is 619 kWh. Compared to the baseline VAWTs' energy generation of 918 kWh, the optimal strategy of arranging the MBSS improves the energy generation by 31.02% . Combining the high C_{P-net} at different TSRs and excellent annual power generation, $n2d0.025c0.05c$ is the relatively optimum case.

2. Analysis of variance

Also, the statistical tool ANOVA (analysis of variance) is adopted to analyze the relationships between independent variables and dependent variable. Table VI lists the results of ANOVA. The p-value and F-value represent the confidence level, with smaller p-values and larger F-values indicating that the corresponding source term is significant. It can be seen that the F-value of Model is 128.57 , 278.97 and 397.92 for TSR = 2.5, 3.25, and 4, respectively. The corresponding p-value is all less than 0.0001 , implying that the regression model is significant, i.e.,

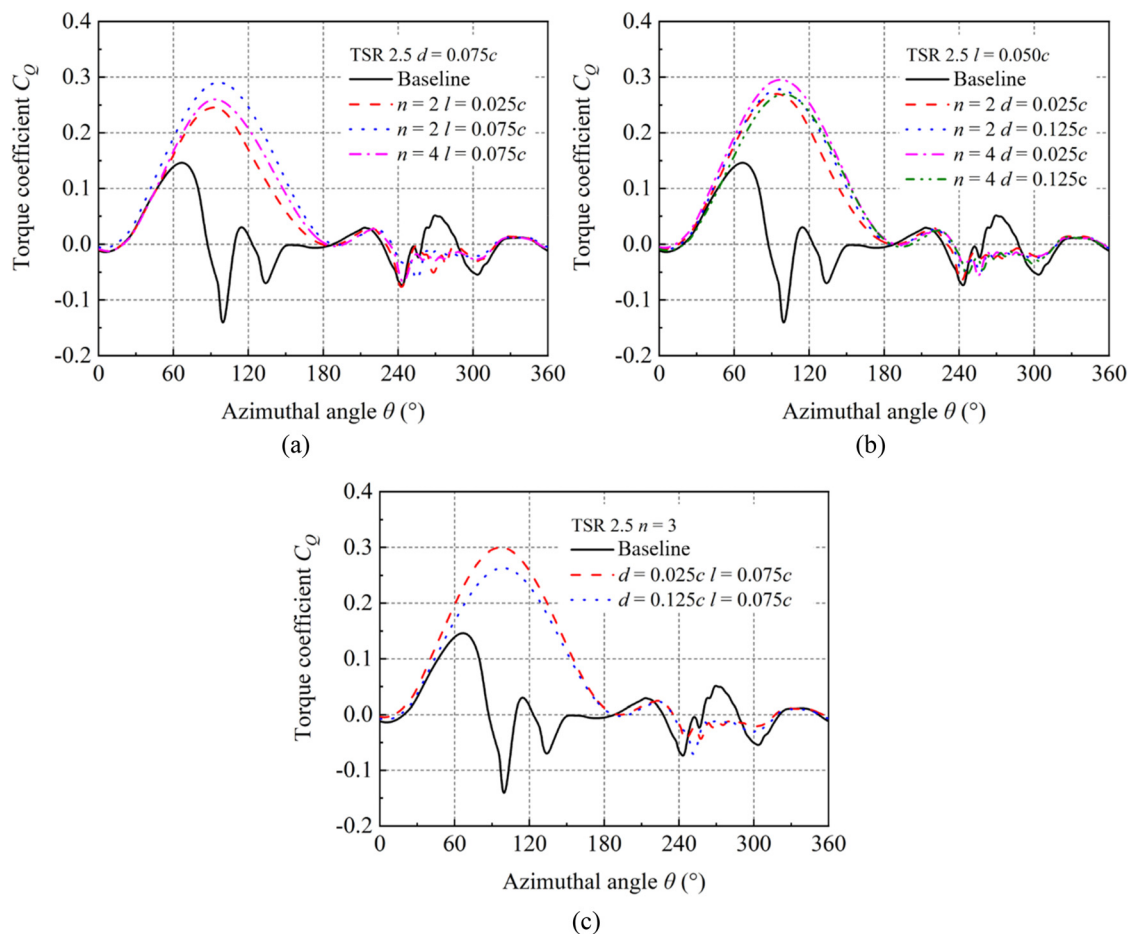


FIG. 9. The variation of the torque coefficient C_Q at TSR = 2.5: (a) Group nl ; (b) Group nd ; and (c) Group dl .

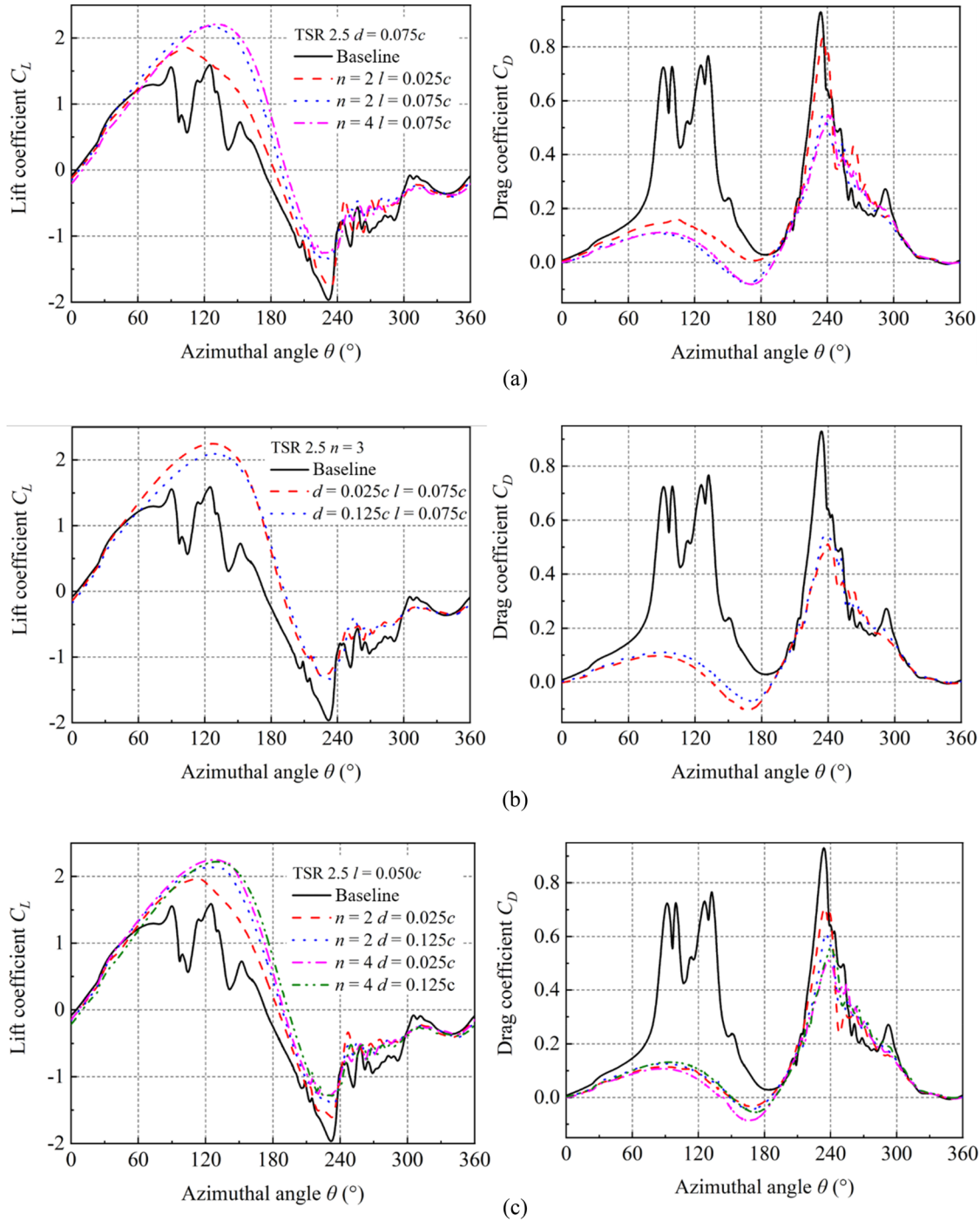


FIG. 10. The variation of the lift coefficient C_L and drag coefficient C_D at TSR = 2.5: (a) Group nl ; (b) Group nd ; and (c) Group dl .

there is only a 0.01% probability that the noise will cause the analysis to be incorrect.

Based on the ANOVA analysis results, the relative importance of the key geometric parameters is revealed. The order of impact under

low and moderate TSRs is: $n > l > d$, while under high TSR it is: $n > d > l$. Notably, the significance of n remains the highest for all TSRs. For low to moderate TSR, the l is more influential than d . At low and moderate TSRs, where significant flow separation occurs on the

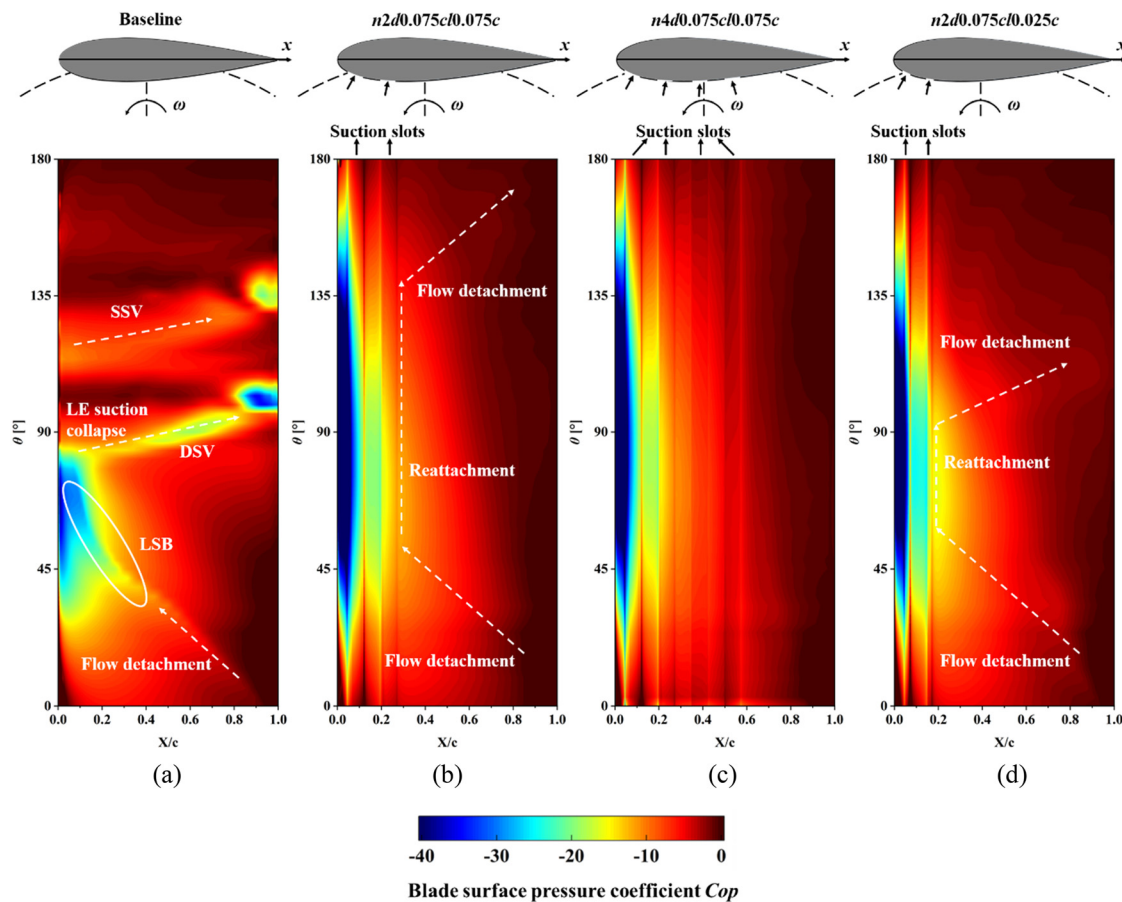


FIG. 11. The cloud plot of the blade surface pressure coefficient C_{op} for group nl at $TSR = 2.5$: (a) baseline; (b) $n2d0.075c/l0.075c$; (c) $n4d0.075c/l0.075c$; and (d) $n2d0.075c/l0.025c$.

blade surface, longer slot lengths imply better control of flow separation, resulting in notable improvements in power production. At high TSR, the importance of d increases and surpasses l . The suction slot's role in regulating the surface flow field becomes less apparent because of the more adherent blade surface flow. Active control consumption dominates the power output of the VAWT, leading to a decrease in the influence of l . In this case, placing the suction slot in a more reasonable location becomes crucial.

Additionally, the interaction between parameters is also noteworthy. For the purpose of discussion, we defined group nl , nd , and dl to evaluate the synergistic effects of the parameters. These groups correspond to scenarios where parameters d , l , and n are individually fixed at intermediate levels. For instance, group nl signifies the case where the parameter d is fixed at the medium level, denoted as $d = 0.075c$. Note that the active control consumption is not considered in the in the following part. The interaction of group nl being stronger than that of group nd and group dl . The reason is that n and l directly reflect the number of single suction slot systems, corresponding to the active control consumption. In summary, a loose suction slot arrangement proves more effective at low TSR, where larger spacing and length of suction slots

enhance the control of severe flow separation. Conversely, a tight suction slot arrangement is more apt for high TSR, featuring smaller spacing and slot length, leading to improved flow attachment and reduced energy consumption in active control.

Table VII lists the convincing well results of the regression model. The R^2_{Adj} is a measure of the amount of variation around the mean explained by the model, adjusted for the number of terms in the model. The R^2_{Pre} is a measure of the amount of variation in new data explained by the model. It can be seen that the R^2_{Adj} reaches 0.9863, 0.9936, and 0.9955 while the R^2_{Pre} reaches 0.9038, 0.9555, and 0.9688 for $TSR = 2.5$, 3.25, and 4, respectively. As a result, the model shows a satisfactory fit in the regression region and reliably predicts new data. The diagnostic plots Fig. 7 show that the regression model is reliable since the predicted values agree well with the actual values.

The cloud plot and the response surface of the effect of the interaction between parameters on C_{P-net} at each TSR is shown in Fig. 8. As can be seen from the cloud plot, there is a clear similarity in the interaction of the different parameters at low and moderate TSRs. For the interaction of nd , the increase in one parameter and the corresponding decrease in the other parameter are favorable for C_{P-net} , which means that the loose suction slot arrangement that enlarges the region of

influence of the suction slot in the boundary layer has a significant effect on improving the performance of the wind turbine blades. The reason for not achieving the best results when the two parameters are increased simultaneously is that some of the suction slots are arranged in the useless area, which will be explained in 3.2.2. Considering group nl , for a fixed suction slot length, the effect on the C_{P-net} is less favorable as the number of suction slots increases. The increased suction slot length is beneficial for the C_{P-net} when the number of suction slots is 2, while when the number of suction slots is 4, the increased suction slots will significantly reduce the C_{P-net} . This is due to the fact that both the length and the number of suction slots can significantly affect active control consumption, and the large power loss from the increased parameter is significantly unfavorable to the C_{P-net} . In the aspect of dl parameter, for the same suction slot length, the larger the distance between suction slots, the smaller the C_{P-net} . At the same distance between suction slots, the C_{P-net} is not sensitive to the change of suction slot length.

The interactions between the individual parameters under $TSR = 4$ show a slightly different trend due to the increase in the influence weight of the parameter d . For the nd condition, the optimal condition can be achieved when both n and d are minimized, implies that the tight suction slot arrangements of the blade LE region favors the net power coefficient. For the nl case, it is beneficial to C_{P-net} to minimize the number of suction slots and the length of the suction slots, when the aerodynamic power enhancement due to the suction slots is no longer able to far outweigh the power input required by the suction slots. As for the ld parameter, the variation of wind turbine power is insensitive no matter how the parameter is changed, and the wind turbine performs well when both parameters l and d are minimized.

In a word, tight and loose suction slot arrangements are suitable for high and low TSRs, respectively. These findings align with the results obtained from ANOVA analysis.

B. Effects of MBLSS parameters on VAWT at $TSR = 2.5$

In 3.1, the analysis of RSM results provides the optimal arrangement strategy for MBLSS, and the effect of key geometric parameters considering active control consumption is also illustrated. This section delves deeper into elucidating the aerodynamic principles associated with the active control provided by MBLSS. The condition of $TSR = 2.5$ is selected because of the drastic flow separation near blades and the boundary layer control effect of MBLSS is more obvious.

1. Aerodynamics parameters

The variation of the instantaneous torque coefficient (C_Q) during one turbine revolution at $TSR = 2.5$ is shown in Fig. 9. The baseline condition torque coefficient curve undergoes drastic fluctuation. The local maxima of torque coefficients occur at approximately 70° , 110° , and 270° , while the local minima values occur at approximately 240° , 270° , and 300° . The significant fluctuation of torque coefficients in the upwind region located in the 0° – 180° region is mainly due to the occurrence of dynamic stall, whereas the fluctuation of torque coefficients occurring in the downwind region located in the range of 180° – 360° is due to the complex blade-vortex interaction. Since the baseline wind turbine is a two-bladed VAWT, the sum of the azimuths of the two blades of the wind turbine during the operation is 360° , which

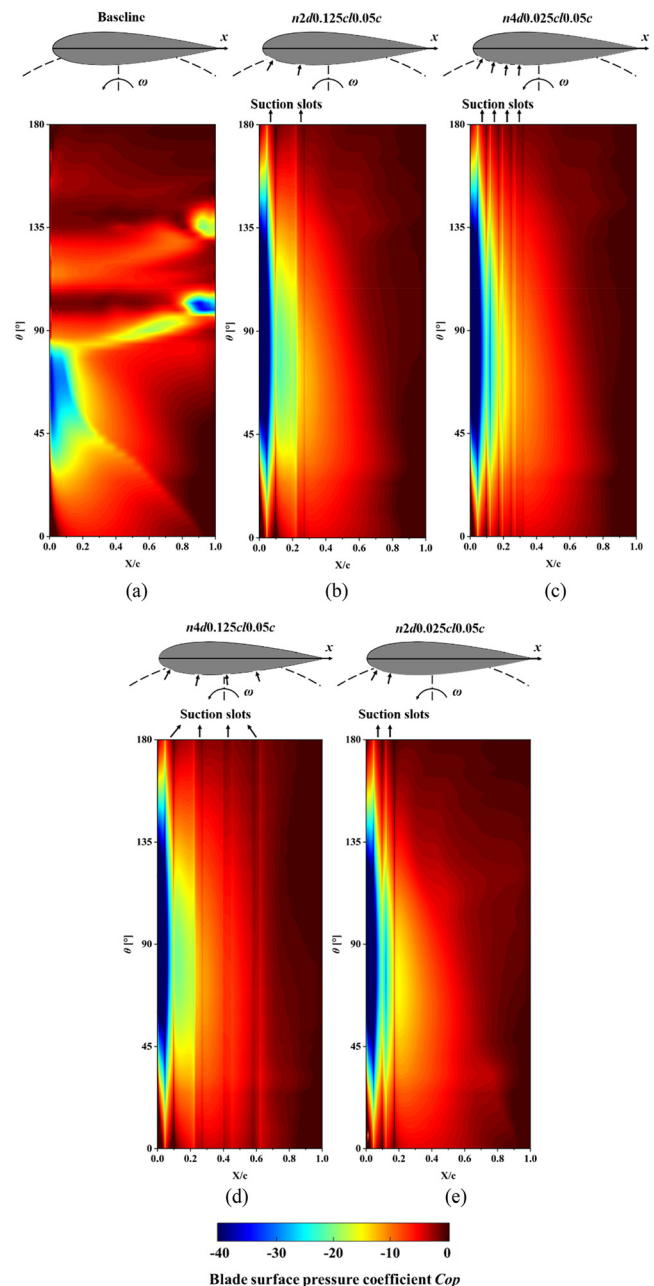


FIG. 12. The cloud plot of the blade surface pressure coefficient Cop for group nd at $TSR = 2.5$: (a) baseline; (b) $n2d0.125c/0.05c$; (c) $n4d0.025c/0.05c$; (d) $n4d0.125c/0.05c$; and (e) $n2d0.025c/0.05c$.

means that when the wind turbine blade 1 is located at the azimuth where the peak of the torque coefficient is located, blade 2 will be located at the corresponding trough. The positive and negative cancellation of the instantaneous torque of the two blades leads to the unsatisfying power output of the baseline turbine observed in Table V.

The MBLSS mitigate the dynamic stall and reduce the intensity of the shedding vortex on blades, and thus the fluctuations in the torque

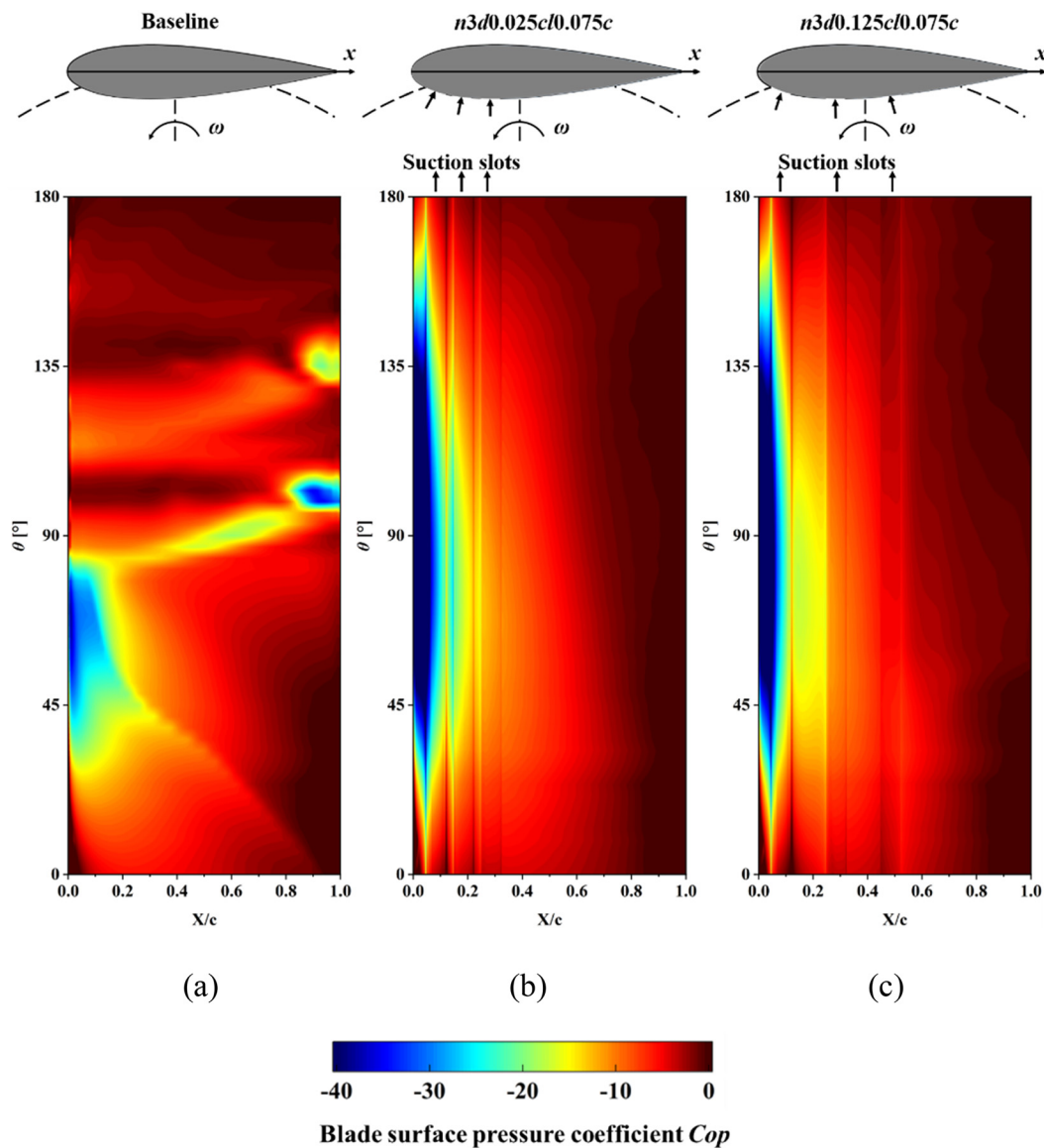


FIG. 13. The cloud plot of the blade surface pressure coefficient C_{op} for group dl at $TSR = 2.5$: (a) baseline; (b) $n3d0.025c/0.075c$; and (c) $n3d0.125c/0.075c$.

coefficient of the wind turbine are mitigated in both the upwind and downwind region. While the baseline blade's C_Q peak at $\theta = 66^\circ$ before decreasing sharply, the MBLSS blades demonstrate a more sustained and elevated instantaneous blade torque. The peaks and corresponding angles differed for each operating condition and the highest peak occurs at $n3d0.025c/0.075c$ case in dl group, which is 104.86% higher than the baseline conditions. For all three groups, the better performing conditions tend to imply a delayed appearance of higher instantaneous torque peaks. Such variations result in power coefficient differences of 30.34%, 17.24%, and 24.81% for cases within group nl , nd , and dl , respectively. It is worth noting that for the relative worse conditions $n2d0.025c/0.05c$ and $n4d0.125c/0.05c$ within group nd , the instantaneous torque coefficients of the two conditions show a subtle difference. The former has an

earlier torque peak at $\theta = 93^\circ$, but also a faster torque drop. The torque coefficient of the latter rises more slowly and peaks at $\theta = 99^\circ$. The torque coefficient peaks of the two cases are not significantly different at 0.13%. This is mainly due to the different regions of influence of the two conditions. $n2d0.025c/0.05c$ has a suction slot that is mainly concentrated at the LE of the blade, while $n4d0.125c/0.05c$ has a much more dispersed suction slot that is able to influence the middle region of the blade. For the flow separation generated during wind turbine operation, the boundary layer suction located at the LE of the blade can protect the development of the suction region at the LE of the blade and prompt the torque coefficient to rise faster. The boundary layer suction at the center of the blade blocks the flow separation from the TE to the LE of the blade and is more influential in the 110° – 180° region. Taking

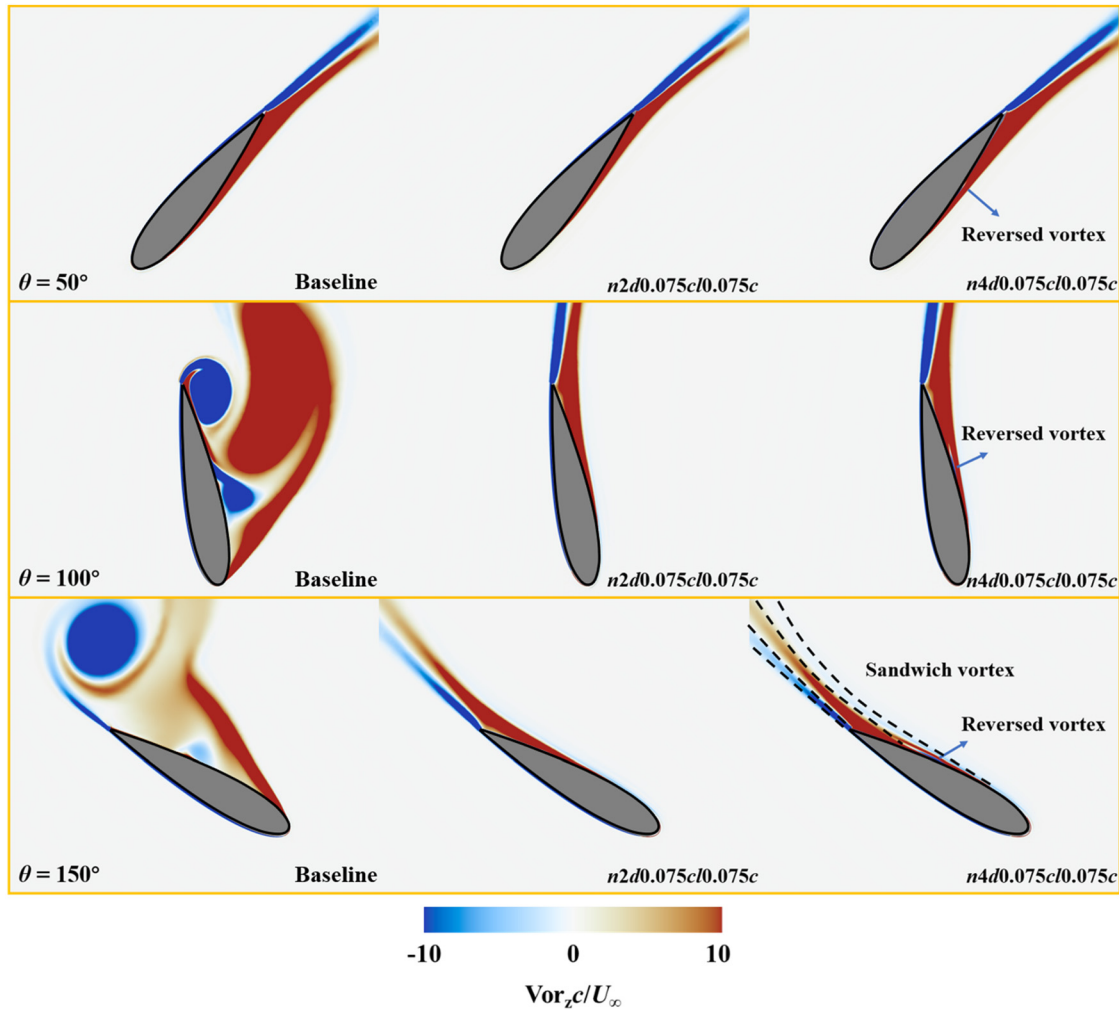


FIG. 14. Contour plots of instantaneous dimensionless vortex.

both into account, the $n4d0.025cl0.05c$ case achieves a leading position in the group. Due to the improved aerodynamic characteristics in the upwind region, the lower vortex shedding intensity and reduced wind speed caused the torque curves in the downwind region to stabilize and produce reverse torque for all cases.

The lift coefficient (C_L) and drag coefficient (C_D) curve in TSR2.5 are shown in Fig. 10. For baseline case, the lift and drag coefficient curves have very significant fluctuations during the revolution of wind turbine, both in the upwind and downwind regions. MBLSS are able to make the C_L and C_D curves smoother, as evidenced by the smooth rise of the C_L in the upwind region and the significant decrease in the C_D over the full revolution. It is worth noting that the variation of the lift and drag coefficient curve is related to the control effect of the multiple suction slots. Better conditions have higher peak lift coefficients and fuller lift coefficient curves. However, for the selected relative worse cases $n2d0.025cl0.05c$ and $n2d0.075cl0.025c$, an early decrease in the lift coefficient of the blade compared with other conditions can be observed. Due to the small number of suction slots and tight slot arrangement

strategy, the boundary layer on the blade surface was not sufficiently controlled. Thus, the boundary layer was not formed in time and further led to significant flow separation, which resulted in an earlier drop in the C_L of the blade than in other conditions. A delayed decrease in drag coefficient was also found for the $n2d0.075cl0.025c$ case.

2. Blade surface pressure coefficient

A more comprehensive understanding of variations in key aerodynamic parameters can be attained by examining alterations in the blade surface pressure coefficient. Figure 11 shows the spatial and temporal evolution of the pressure coefficients on the inside of the blade for the group nl . For baseline, it can be seen that the flow detachment is gradually generated from the TE of the blade and then gradually moves forward with the increasing of the blade azimuth angle. When the detachment fully develops, the negative pressure zone at the LE of the blade will continue to develop and laminar separation bubbles (LSB) will be observed. Two distinct vortex detachment points can be

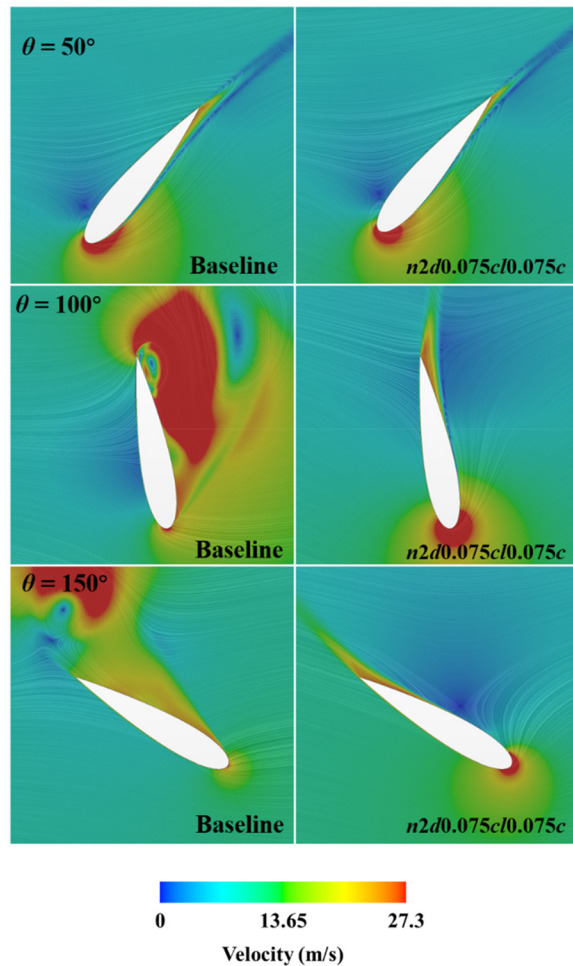


FIG. 15. Instantaneous velocity distribution around the blades at TSR = 2.5.

observed. When the negative pressure zone collapses and LSB breaks up at an azimuthal angle of about 80° , the resulting dynamic stall vortex (DSV) then moves toward the TE of the blade and off the trailing end of the blade. At around 120° , a secondary dynamic stall vortex (SSV) is generated from the LE of the blade and rapidly breaks up and moves backward. Such a phenomenon corresponds to the drastic change in the instantaneous torque coefficient in Fig. 9.

The presence of the suction slots inhibits the development of LSB and make sure that the negative pressure zone can develop until the end of the rotation. A negative pressure zone is formed at the LE of the suction slot. The suction interrupts the development of LSB, which inhibits the generation of DSV and allows the blade to avoid dynamic stall, resulting in a smoother power output. The best-performing case $n2d0.075c0.075c$ in group *nl* has reasonable distance between slots and desirable slot length, which makes the ability in the rectification of the flow to be fully utilized. The laminar separation is suppressed, and the overall flow of the flow field is more attached. Due to the small length of the suction slot for the $n2d0.075c0.025c$ condition, the distribution of the suction slots group is close to the LE region of the blade, and the control effect in the process of vortex forward development

cannot be fully realized. As reflected in the pressure coefficient distribution diagram, the flow separation point moving toward the LE gets to the suction slots at $\theta = 60^\circ$. The flow around the blade is attracted by the suction slot, flow reattachment occurs. When the $\theta = 90^\circ$, the flow separation point arises again and gradually develops toward the TE of the blade, and the blade wall flow undergoes reattachment, which corresponds to the instantaneous torque coefficient decrease in the torque coefficient curve. For the $n4d0.075c0.075c$ case, the control efficiency of a single suction slot is rather lower despite the fact that there are more suction slots, which is due to the gradual development of the strength of the roll-up vortices induced by the suction slots, shielding the suction control effect of the MBLSS to a certain extent, which will be explained in detail in Sec. III B 3.

In group *nd*, Fig. 12 illustrates a well-established negative pressure zone at the LE region of the blade for all cases, indicating a mitigation of the flow separation trend on the blade surface. The LSB progressively forms from the TE region of the blade and is initially weakened at the last suction slots. This phenomenon enhances the adherence of the flow field on the wind turbine blade surface, particularly in high angle of attack (AoA) conditions prone to dynamic stall. An ample number of suction slots are strategically placed at the LE region of the blades, effectively addressing potential separation issues. The $n2d0.125c0.05c$ and $n4d0.025c0.05c$ cases, featuring well slot distribution strategies, both exhibit a favorable influence on the performance of the wind turbine. However, the aerodynamic power coefficients for the $n2d0.125c0.05c$ and $n4d0.025c0.05c$ cases are 0.2879 and 0.3242, respectively, while the corresponding net power coefficients are 0.2333 and 0.1723. Although the aerodynamic power coefficients are higher for the $n4d0.025c0.05c$ case, the extra suction slot also means higher active control consumption, reducing the total output of this strategy. For the $n4d0.125c0.05c$ condition, the suction slots closest to the TE of the blade does not have a significant control effect, which leads to a certain degree of wasted control efficiency. For the $n2d0.025c0.05c$ case, due to the extremely small spacing, the control effect of MBLSS is concentrated on the LE of the blade, and the LSB is not controlled most efficiently during their forward development, thus they continue to develop around $\theta = 120^\circ$ and produce a slight flow separation, which leads to a degradation of the aerodynamic power coefficient. In summary, the active control strategy of arranging the MBLSS at the LE of the blade, i.e., the region between $X/c = 0c$ and $X/c = 0.3c$, where flow separation is likely to occur with a fixed suction slot length, provides a larger enhancement of the aerodynamic coefficient of the wind turbine. Considering the energy consumption of active control, reducing the number of suction slots and spreading out the suction slots are beneficial to the net power output of the wind turbine.

For the cloud plot of the blade surface pressure coefficient for group *dl* shown in Fig. 13, the best performing case, $n3d0.025c0.075c$, and the worst case, $n3d0.125c0.075c$, had similar control effects at the LE of the blade, which adsorbed the streamlines well above the blade. However, the increased pitch also leads to poor control, again because the distance is too long, leading to vortices beyond the influence of the suction slot and further formation of roll-up vortices that stratify the flow field. This is consistent with the previously mentioned conclusion that concentrating the suction slots at the LE of the blade is more effective.

3. Vorticity and velocity distributions

Section III B 2 delves into the spatial and temporal evolution of pressure coefficients on the inner side of the blade, yet visualizing the

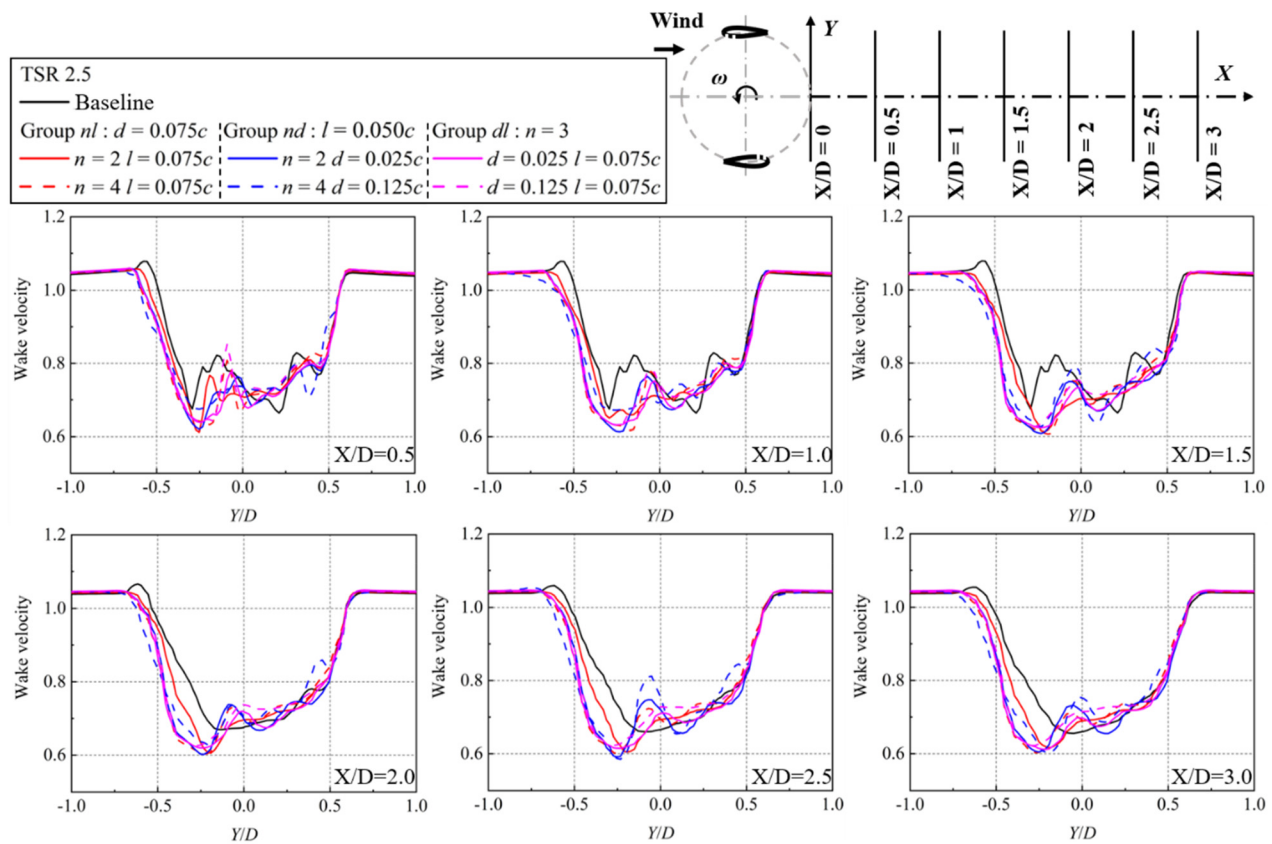


FIG. 16. Normalized mean near wake velocity profiles of the studied VAWT at $TSR = 2.5$.

development of vortices on the outer surface of the blade is not feasible. The vorticity profiles of group nl used to visualize the effect of the MBLSS are discussed in this part due to the importance of n and l declared in the ANOVA.

Three typical conditions, baseline, a well condition $n2d0.075cl0.075c$, and a worse condition $n4d0.075cl0.075c$, are compared in Fig. 14. Similar to the pressure coefficient spatial and temporal evolution figures, the flow around baseline's blades exhibits very

significant flow separation, with significant vortex shedding around 90° and 130° . In contrast, $n2d0.075cl0.075c$ shows no significant vortex shedding process, and the flow around the blade is more attached, due to the adsorption effect of the MBLSS. The attached flow causes the vortex that would otherwise have developed from the separation point at the LE of the blade toward the TE to be canceled out, resulting in a more backward separation point of the blade. It also results in the vortex developing at a reduced distance and thus unable to generate a stable shedding vortex. The lag of the separation point is also reflected in the $n4d0.075cl0.075c$ case, but the lag of the separation point is regulated by the leading-edge suction slot with a shorter lag distance, which leads to the vortex development in advance and beyond the influence range of the TE suction slot. Within the influence range of the TE suction slot, the vortices that originally attracted the flow to the inward side due to the leading-edge vortices being far away from the wall, the suction to the inward side led to the generation of reverse vorticity, which rapidly developed backward. When the AoA is large, the leading-edge vortex has a larger space for development and thus wraps the reverse vortex inward and gradually neutralizes the reverse vortex and develops backward with weaker intensity. When the AoA is small, because the leading-edge vortex returns to the influence area of the suction slot, the reverse vortex generated by the TE suction slot will be fully developed, and thus, a sandwich cake type vortex is formed at the blade wake.

The instantaneous velocity distributions around the blade for both the baseline condition and the optimized condition

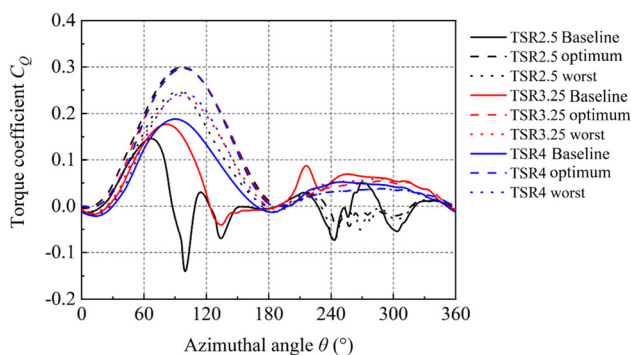


FIG. 17. The variation of the instantaneous torque coefficients for the baseline with the optimum and worst improvement conditions for each TSR.

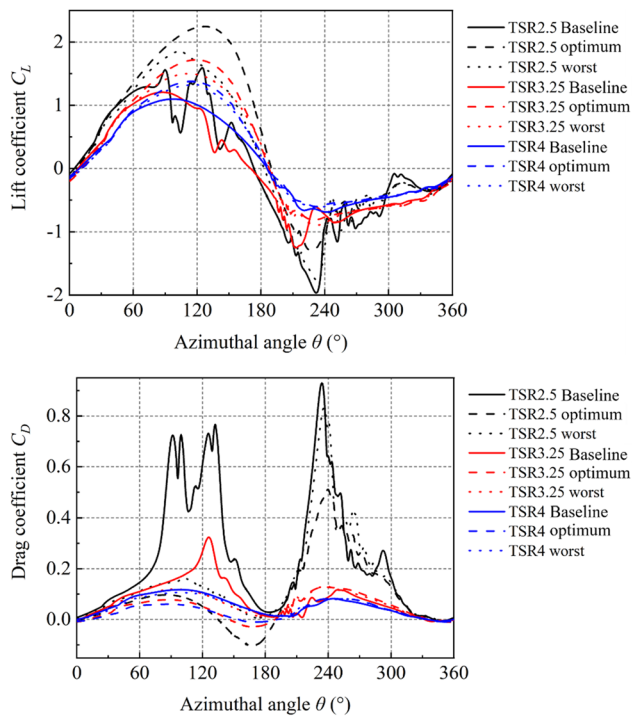


FIG. 18. The variation of the instantaneous lift and drag coefficients for the baseline with the optimum and worst improvement conditions for each TSR.

$n2d0.075lc0.075c$ within the group nl are further illustrated for $TSR = 2.5$ in Fig. 15. At $\theta = 50^\circ$, the baseline case exhibits the formation of the blade wall boundary layer, leading to reverse airflow due to a negative pressure gradient within the boundary layer. This reverse flow continues to develop, resulting in significant vortex shedding at $\theta = 100^\circ$. At $\theta = 150^\circ$, the instantaneous AoA decreases, facilitating the reformation of the boundary layer and the reattachment of the flow to the surface of the blades. In contrast, for the $n2d0.075lc0.075c$ case with superior control, the presence of the suction slots at an azimuth angle of 50° continually disrupts the boundary layer, compelling the flow on the blade surface to reattach multiple times. This overcoming of the negative pressure gradient within the boundary layer leads to the narrowing of the relative acceleration zone of the airflow at the LE of the blade. This effective control persists as the azimuth angle increases, maintaining the relative acceleration zone at the LE and eliminating vortex shedding. These findings align with the analysis presented in the blade surface pressure coefficient distribution in Fig. 13.

4. Wake velocity profile

The tight arrangement strategy of VAWTs is an important development direction for wind farms, which has received extensive attention from scholars.^{53,54} What plays a controlling role on the tight row arrangement of VAWTs is the near wake flow of prostate wind turbines. The near wake flow of VAWTs has not been deeply studied for the time being. According to Lam *et al.*,⁵⁵ although 2D CFD simulations cannot obtain the evolutions of tip vortices and the effect of the flows come into the wake from the top and bottom of the blades,

which leads to unstable wake expansion in the far wake region, it can still derive reasonable wake characteristics in the near wake region due to the more incomplete vortex diffraction.

Figure 16 illustrate the differential of near wake profiles between the representative MBLSS cases with the baseline within each interaction group. MBLSS has a significant impact on the VAWT near wake profile. A significant decrease in the mean wake velocity is observed in the region from $Y = -0.7D$ to $-0.15D$, while in the region from $Y = -0.15D$ to $0.5D$ the main effect of MBLSS is a more violent fluctuation. Outside the region from $Y = -0.7D$ to $0.5D$, the near wake velocity of VAWT is not much affected, which means that for the VAWT arrays, the downstream VAWT placed outside the region of $Y = -0.7D$ to $0.5D$ will be able to avoid the unfavorable influence of the MBLSS effect of the upstream VAWT.

C. Effects of MBLSS parameters on VAWT at different TSRs

As mentioned previously in 3.1.1, the effect of the same strategy for suction slot arrangement on the aerodynamic characteristics of VAWTs at different TSRs shows a similar trend. Among all the suction slot arrangement strategies, the highest C_p of VAWT was found under the case of $n3d0.025cl0.075c$. It is the aerodynamic optimum case and leads to aerodynamic performance increases of 785.74%, 92.50%, and 60.54% for low, moderate and high TSR conditions, respectively. The worst aerodynamic performance conditions are different. The $n2d0.075cl0.025c$ case has the worst aerodynamic performance increases of 496.48% and 55.72% at moderate and lower TSRs, respectively. While for high TSR, the worst case is $n3d0.125cl0.025c$, and the improvement of C_p is 21.99%.

1. Aerodynamic parameters

The instantaneous torque coefficients for the baseline with the optimum and worst improvement conditions for each TSR are shown in Fig. 17.

For the baseline cases, due to the difference in the degree of aerodynamic separation at different TSRs, the curves for $TSR = 4$ are fuller than those for $TSR = 2.5$, while reaching higher peak instantaneous torque coefficients at larger azimuthal angles. Such differences diminish with the control of the airfoil flow field by the multiple suction slots. Similar curve peaks and corresponding azimuthal angle can be observed under the worst improvement conditions. For the optimum condition $n3d0.025cl0.075c$, the peak values of the instantaneous torque coefficients occur at 100° azimuth. This indicates that the instantaneous torque coefficients in the upwind region will be similar with the same MBLSS control strategy. The curves in the downwind region are more chaotic. For the case of low TSR, obvious fluctuations can be observed, which is due to the fact that the rotational speed of the VAWT is slower in the case of low TSR, and the wind turbine blades operate at a lower relative speed and a larger AoA in the downwind region, whereas, for moderate and high TSRs, higher blade relative speeds allow the wind turbine blades to also generate positive torque coefficients and capture energy from the incoming wind.

A comparison of lift coefficient and drag coefficient between operating conditions at different TSRs is shown in Fig. 18. In the lift coefficient curve, the active control of multiple suction slots will make the lift coefficient curve less fluctuating and fuller. The peak lift coefficient for the low TSR condition will be significantly higher than the

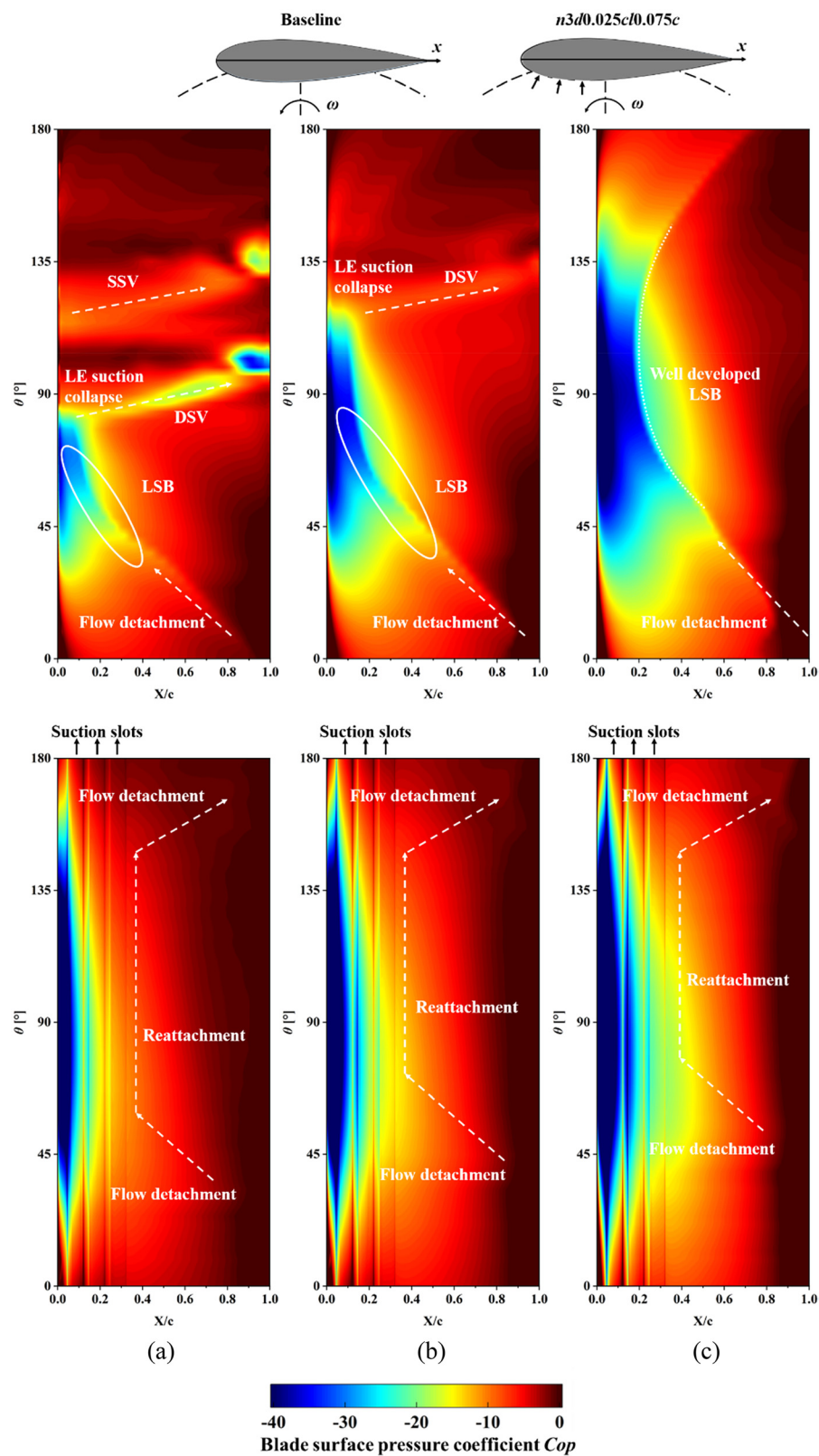


FIG. 19. The cloud plot of the blade surface pressure coefficient C_{op} for baseline and optimum condition: (a) $TSR = 2.5$; (b) $TSR = 3.25$; and (c) $TSR = 4$.

28 November 2025 04:17:12

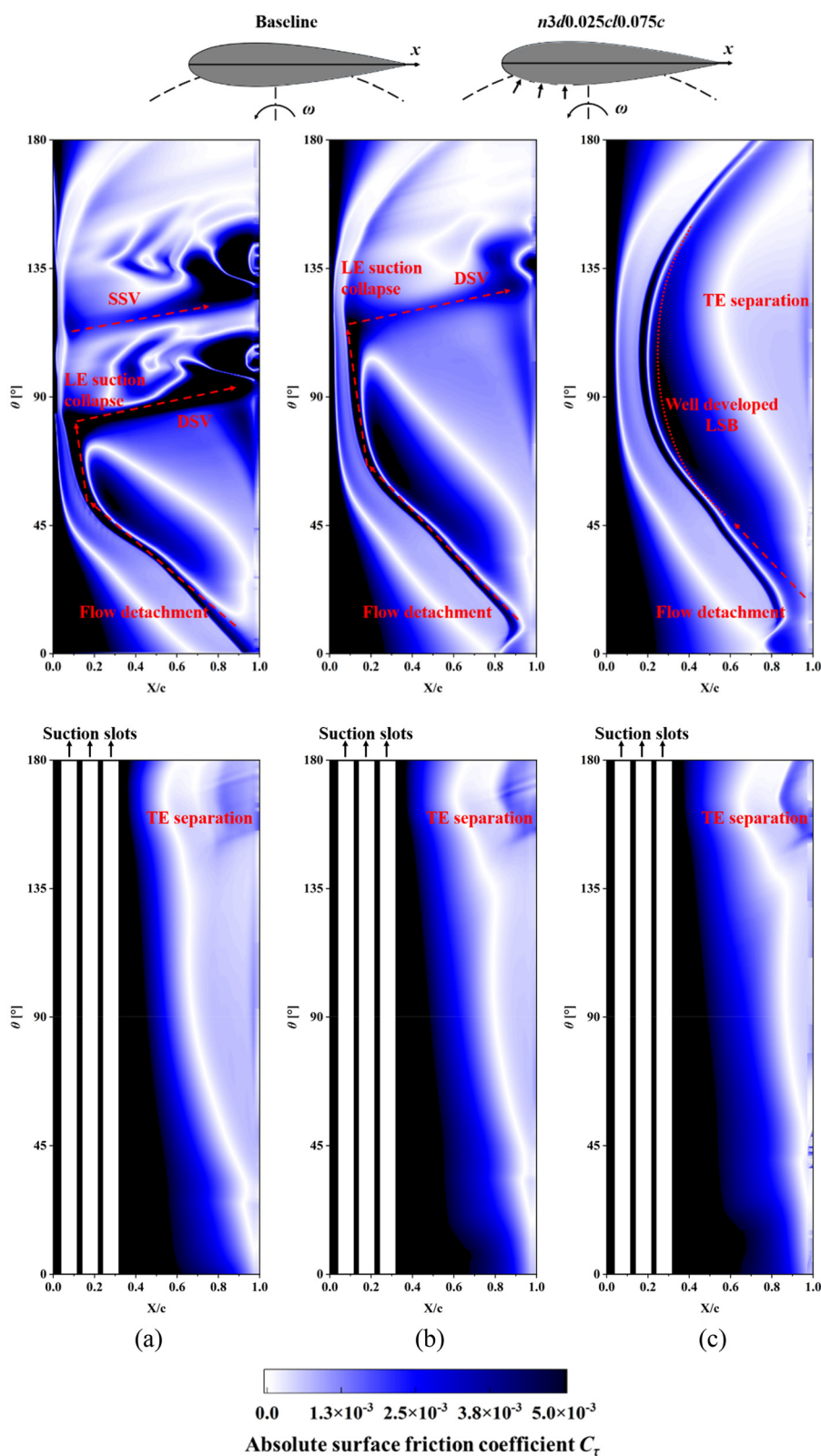


FIG. 20. The cloud plot of the absolute surface friction coefficient C_τ for baseline and optimum condition: (a) TSR = 2.5; (b) TSR = 3.25; and (c) TSR = 4.

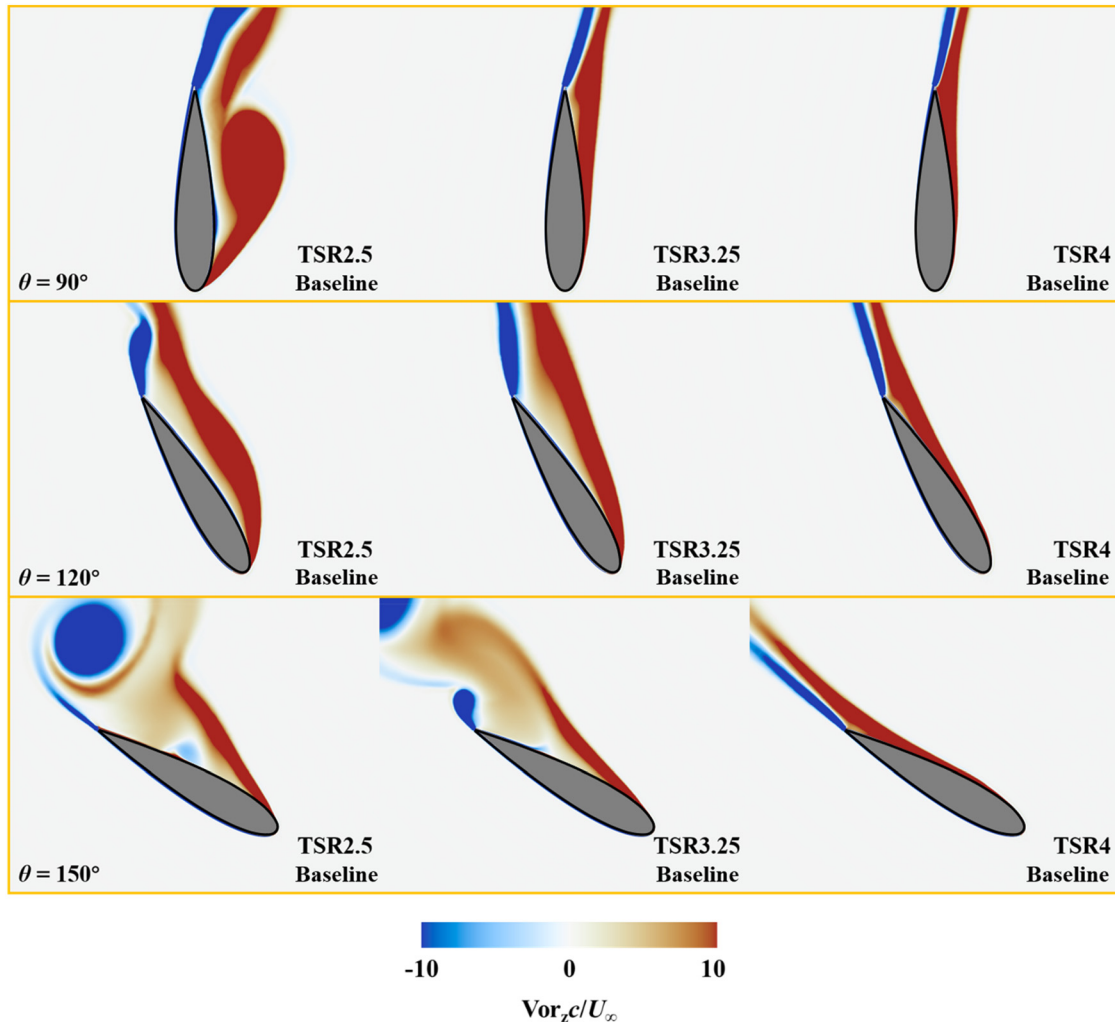


FIG. 21. Contour plots of instantaneous dimensionless vortex for baseline.

peak lift coefficient for the high TSR condition, which is due to the larger AoA experienced by the blades during wind turbine operation at the low TSR. In the comparison of the optimal control conditions for each TSR, it can be found that the variation trend of the lift coefficient in the upwind region is very similar to that of the AoA. Under the control of multiple suction slots, the drag coefficients of each working condition in the first half of the cycle are significantly reduced. In the downwind region, due to the complex blade-vortex interaction, the peak value of the drag coefficient at the low TSR decreases significantly and retains a large fluctuation characteristic, and the drag coefficients at the moderate and high TSRs tend to be smoothed out, but the peak values do not have a significant difference.

2. Blade surface pressure coefficient and absolute friction coefficient

The spatiotemporal distribution of pressure coefficients on the blade surface of VAWT for each TSR is shown in Fig. 19. The flow

separation phenomena, i.e., laminar separation bubbles, dynamic stall vortices, TE separation, etc., that occur in each case are controlled by the multiple suction slots suction strategy. The three suction slots under the optimal condition multiple suction slots arrangement strategy have different effects. The main effect of the suction slot near the TE is to hinder the development of LSB toward the LE of the blade. This is due to the fact that the development of laminar flow separation bubbles toward the LE is interrupted by the suction slot. With the failure of negative pressure development, the flow is forced to reattach at the TE of the suction slot, where the TE separation is small enough to generate a violent stall vortex. The suction slot near the LE of the blade is then responsible for reattaching the separated flow generated at the point where the LE of the blade separates at high angles of attack to the blade. The reason is the suction slot near the LE of the blade is also closer to the flow separation point, and the wall flow is not out of the control range of the suction slot before the flow is attached by pumping out low-energy fluids and allowing the inflow of high-energy fluids from the outside. The middle suction slot is mainly used to extend the

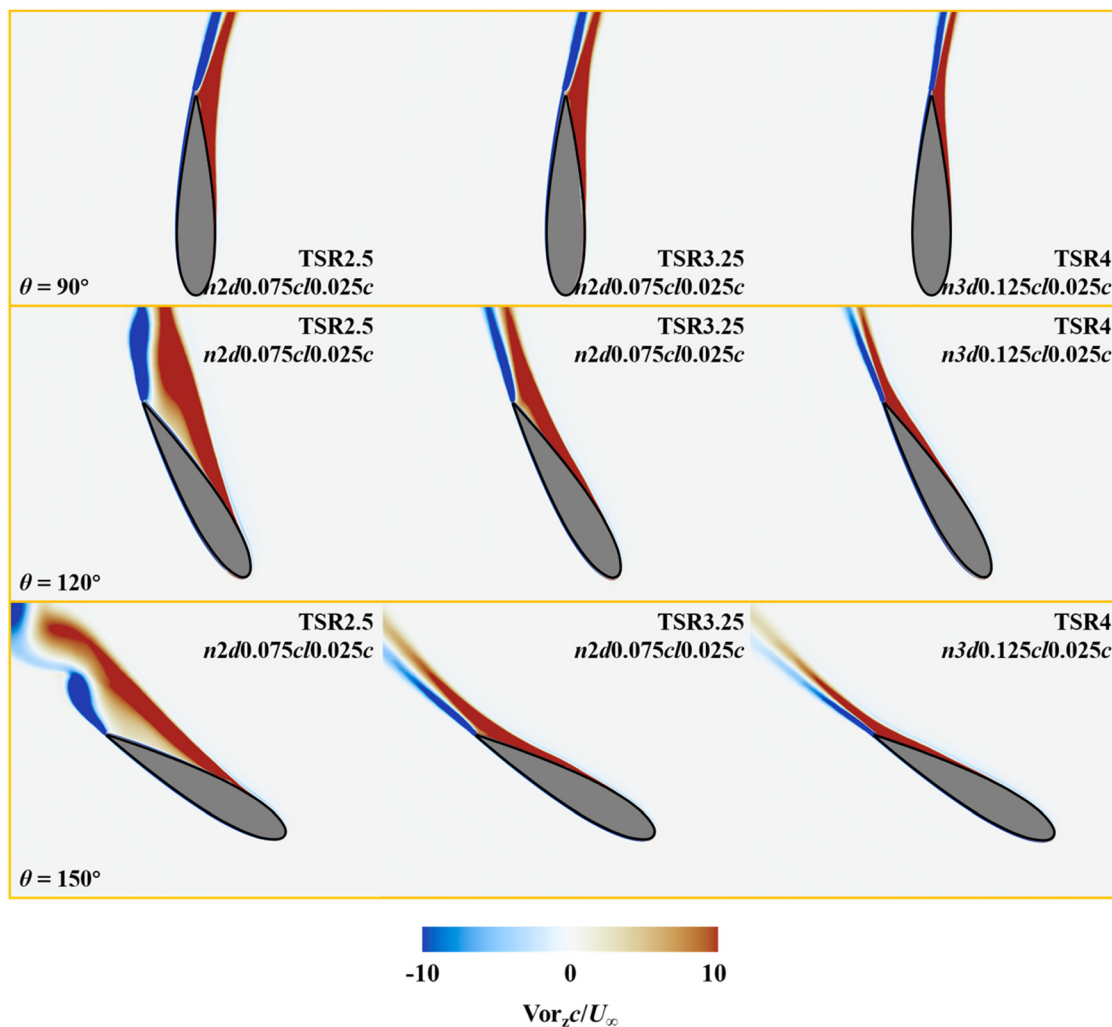


FIG. 22. Contour plots of instantaneous dimensionless vortex for worst condition.

control area. Under the control of multiple suction slots, the dominant flow separation phenomenon is mainly TE separation, which has little effect on the drag coefficient of wind turbine blades.

The spatiotemporal diffraction of the absolute surface friction coefficient C_f on the blade surface presented in Fig. 20 can be added to illustrate the movement of the separation point as well as the development of vorticity. For the baseline conditions at each TSR, it can be clearly observed in the figure that the flow separation point on the inside of the blade gradually develops from the TE of the blade to the LE of the blade as the blade AoA increases. As the AoA gradually increases and surpasses the dynamic stall angle, the separation point swiftly shifts to the TE of the blade, coinciding with the collapse of the leading-edge suction region. This is accompanied by pronounced flow separation, leading to the formation of a dynamic stall vortex. For the high TSR condition with small AoA, the separation zone at the TE of the blade with small degree of flow separation can be fully developed. For the optimal multiple suction slots arrangement strategy, the absolute surface friction coefficients at different blade TSRs show similar

trends. Due to the suction effect, a tangential flow of air is generated in the region from the TE of the suction slots to the TE of the blade, and such a tangential flow region decreases with the increase in the blade azimuth angle. The surplus region is predominantly occupied by the suction area at the TE of the blade. Given that the degree of flow separation in the TE suction region is considerably smaller than in the dynamic stall region, the spatial dominance of the TE suction region proves advantageous for turbine performance.

3. Vorticity distributions

Blade vortex plots for baseline conditions at different TSRs show that in Fig. 21, the blade flow separation is more drastic at low TSRs than at high TSRs. This corresponds to the variation curve of the AoA of the VAWT blade during the operation of the wind turbine. The degree of flow separation decreases with increasing TSR. At low TSRs, flow separation is pronounced, leading to the generation of dynamic stall and significant vortex shedding. Moderate TSRs exhibit a slightly

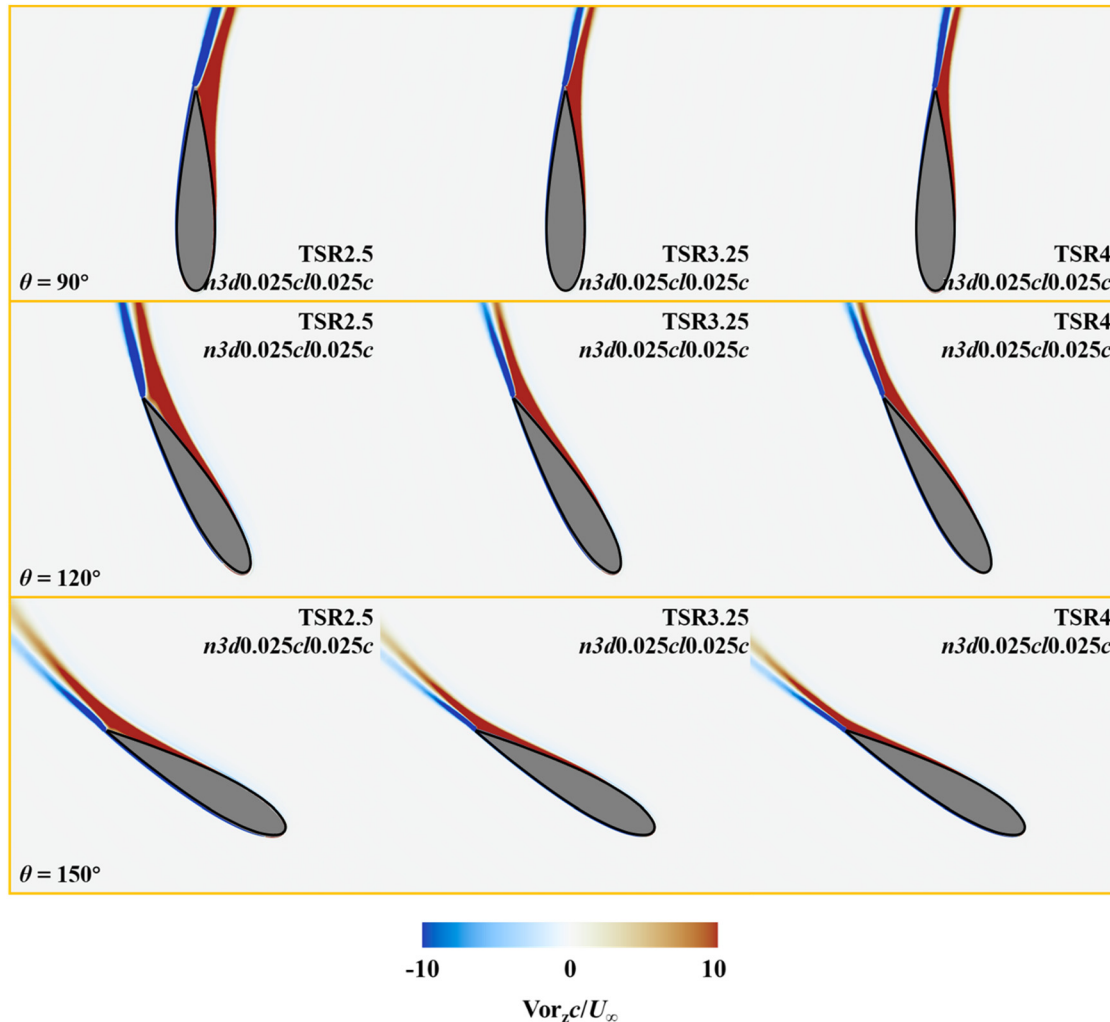


FIG. 23. Contour plots of instantaneous dimensionless vortex for optimum condition.

weaker degree of flow separation and less intense vortex shedding. In contrast, high TSRs result in overall better flow attachment around the blade, minimizing the significance of flow separation.

The blade vortex plots for the worst case with different TSRs are displayed in Fig. 22. Under the worst-case control strategy, the multiple suction slots have a moderating effect on the flow near the blades. For low tip ratios, the worst-case control strategy significantly reduces the vorticity in the vicinity of the blades, but significant flow separation can still be observed. Nevertheless, the suction slot control still mitigates the flow separation and avoids the generation of dynamic stall vortices. For moderate TSR, the worst control strategy resulted in flow attachment near the blades of the vertical axis wind turbine without significant flow separation. For high TSR, the worst-case control strategy also resulted in a more adherent flow near the blades. However, for the already relatively adherent air flow at high TSRs, the large suction slots allow a slight reverse vortex to build up and dissipate during backward progression, without developing a sandwich wake.

The vortex diagrams of the blades for optimal conditions at different TSR are displayed in Fig. 23. The suction control with multiple suction slots has a significant effect on the regulation of vertical axis wind turbine blades. This is mainly reflected in the fact that the suction control with multiple suction slots makes the flow near the wind turbine blades more adherent. The flow separation near the wind turbine blades is greatly reduced for both low and moderate TSRs, similar to that for high TSR. The case $n3d0.025cl0.075c$, as the optimal control strategy for all TSRs, has a good controlling effect on wind turbine operation under all operating conditions.

4. Wake velocity profile

The near wake mean velocities for the baseline case and the optimal MBLSS control case for each TSR are shown in Fig. 24. Due to the improvement of the flow field around the wind turbine blades by the MBLSS, the wind turbine C_p is significantly increased, and thus the wind turbine captures more energy from the incoming wind and

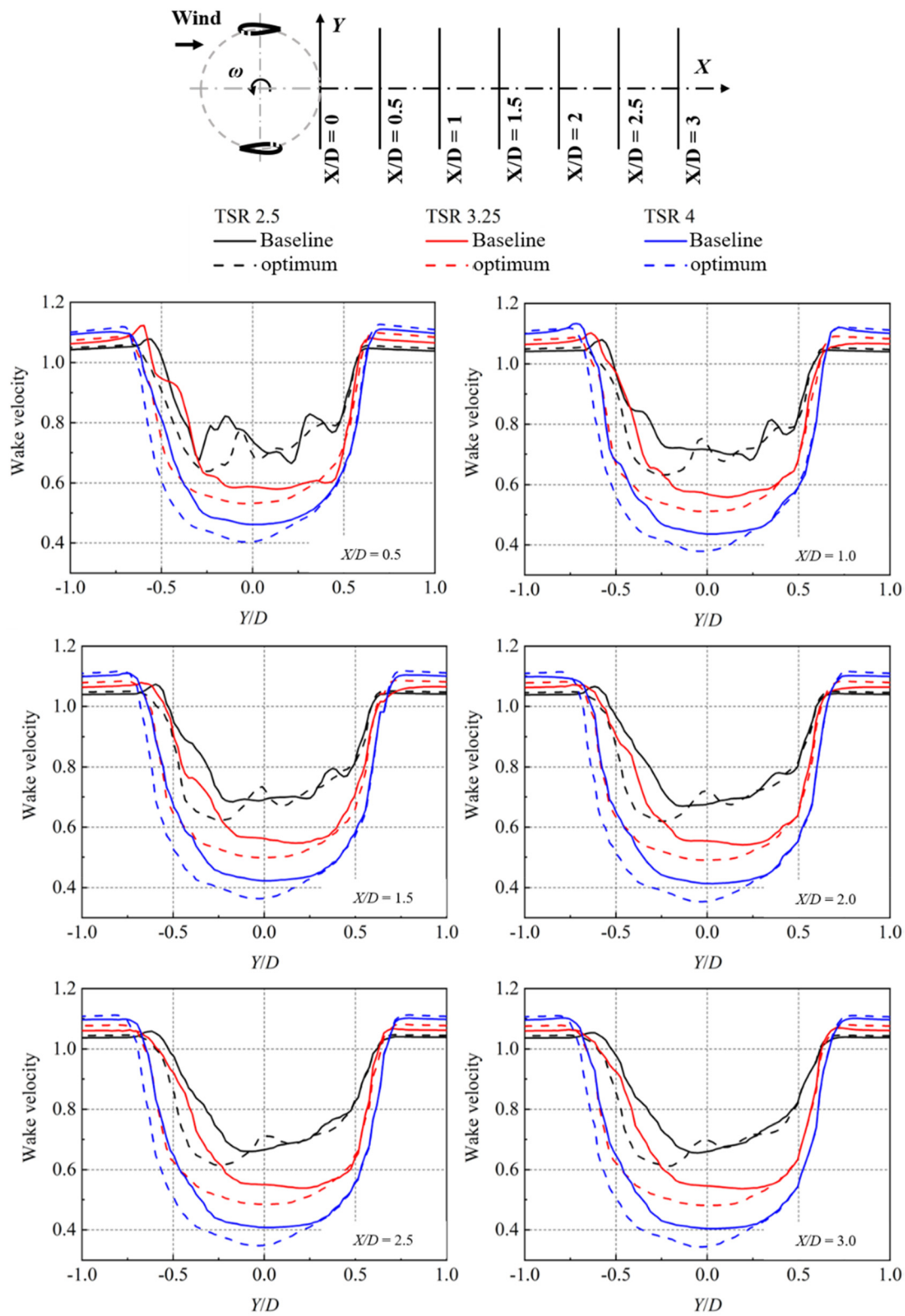


FIG. 24. Normalized mean near wake velocity profiles of the reference VAWT for baseline and optimum condition for each TSR.

reduces the mean wake velocity. However, it can be observed that the near wake profiles at all TSRs have significant changes when Y belongs to $-0.4D$ to $0.3D$, whereas there is no significant difference between the wake profiles for the optimal control condition and the baseline condition in the interval from $0.3D$ to $1D$. This also implies that for MBLSS strategy, the second VAWT near the wake should be located in the area above $0.3D$ in the Y direction of the first VAWT to avoid the suction slots wake effect.

IV. CONCLUSIONS

In the present study, transition SST 4-equations turbulent model is adopted in CFD simulations to investigate the effect of MBLSS on the power performance of VAWTs. Three key parameters, i.e., number of slots, distance between slots, and length of slots, are studied through response surface method across a wide range of TSRs. The flow pattern around turbine blades and turbine wake are compared to examine the aerodynamics and particularly close wake characteristics of VAWTs. The main findings are as follows:

- MBLSS can significantly increase the power output of VAWTs at all TSRs. The maximum improvement in the C_{Pnet} of VAWT is 0.1872 at $TSR = 2.5$, allowing VAWTs to achieve performance levels similar to those at high TSRs. This avoids the detrimental effects on the main structure of the wind turbine.
- The aerodynamic optimum case, represented by $n3d0.025c/0.075c$, leads to aerodynamic performance increases of 785.74%, 92.50%, and 60.54% for low, moderate, and high TSR conditions, respectively. Simultaneously, the relatively optimum case, denoted as $n2d0.025c/0.05c$, resulted in a remarkable 31.02% increase in annual power generation in the test set.
- Tight and loose suction slots arrangement strategies are suitable for relatively low TSR and high TSR, respectively. A tight strategy is necessary to achieve adequate control of dramatic flow separation at low TSR, while a loose strategy can make the active control more reasonable.
- The effective arrangement area of the suction slots is located at $0c-0.3c$ of the LE of the blade. When the suction slot is more than $0.3c$ away from the LE of the blade, the power enhancement of the wind turbine brought by the suction slot can't offset the power loss it needs, and the added suction slot becomes an ineffective suction slot.
- MBLSS has a significant impact on the VAWT near wake profile. The near wake region of the wind turbine under the optimal aerodynamic improvement control strategy with different TSRs decrease considerably and is mainly concentrated in the region from $Y = -0.7D$ to $Y = 0.5D$.

SUPPLEMENTARY MATERIAL

See the [supplementary material](#) for the CFD accuracy validation, which is not elaborated in the main manuscript for brevity, including plat suction slot validation and reference turbine validation.

ACKNOWLEDGMENTS

The financial supports from the National Key R&D Program of China (No. 2023YFE0120000), Guangdong Basic and Applied Basic Research Foundation (No. 2023A1515240054), National Natural Science Foundation of China (Nos. 52122110, 42076210, and 42306226),

Shuguang Program of Shanghai Education Development Foundation and Shanghai Municipal Education Commission (No. 19SG10), Innovation Program of Shanghai Municipal Education Commission (No. 2019-01-07-00-02-E00066), and Oceanic Interdisciplinary Program of Shanghai Jiao Tong University (No. SL2020PT201) are gratefully acknowledged.

AUTHOR DECLARATIONS

Conflict of Interest

The authors have no conflicts to disclose.

Author Contributions

Rui Zhang: Conceptualization (equal); Data curation (equal); Formal analysis (equal); Investigation (equal); Methodology (equal); Software (equal); Validation (equal); Visualization (equal); Writing – original draft (equal); Writing – review & editing (equal). **Limin Kuang:** Conceptualization (equal); Writing – original draft (equal); Writing – review & editing (equal). **Yu Tu:** Writing – original draft (equal); Writing – review & editing (equal). **Zhikun Dong:** Writing – review & editing (equal). **Huan Ping:** Writing – review & editing (equal). **Kai Zhang:** Project administration (equal); Supervision (equal). **Zhaolong Han:** Funding acquisition (equal); Resources (equal). **Dai Zhou:** Funding acquisition (equal); Project administration (equal); Resources (equal); Supervision (equal). **Yan Bao:** Project administration (equal); Supervision (equal).

DATA AVAILABILITY

The data that support the findings of this study are available from the corresponding author upon reasonable request.

REFERENCES

- ¹IEA, *World Energy Outlook 2022* (IEA, Paris, 2022).
- ²Y. Yan, E. Avital, J. Williams, and J. Cui, "Aerodynamic performance improvements of a vertical axis wind turbine by leading-edge protuberance," *J. Wind Eng. Ind. Aerodyn.* **211**, 104535 (2021).
- ³M. Ghasemian, Z. N. Ashrafi, and A. Sedaghat, "A review on computational fluid dynamic simulation techniques for Darrieus vertical axis wind turbines," *Energy Convers. Manage.* **149**, 87 (2017).
- ⁴A. Abdolatifar and S. M. H. Karimian, "A comprehensive three-dimensional study on Darrieus vertical axis wind turbine with slotted blade to reduce flow separation," *Energy* **248**, 123632 (2022).
- ⁵O. S. Mohamed, A. A. Ibrahim, A. K. Etman, A. A. Abdelfatah, and A. M. R. Elbaz, "Numerical investigation of Darrieus wind turbine with slotted airfoil blades," *Energy Convers. Manage.* **X** **5**, 100026 (2020).
- ⁶S. Yoo and S. Oh, "Flow analysis and optimization of a vertical axis wind turbine blade with a dimple," *Eng. Appl. Comput. Fluid Mech.* **15**, 1666 (2021).
- ⁷D. De Tavernier, C. Ferreira, A. Viré, B. LeBlanc, and S. Bernardy, "Controlling dynamic stall using vortex generators on a wind turbine airfoil," *Renewable Energy* **172**, 1194 (2021).
- ⁸Y. Yan, E. Avital, J. Williams, and J. Cui, "CFD analysis for the performance of micro-vortex generator on aerofoil and vertical axis turbine," *J. Renewable Sustainable Energy* **11**, 043302 (2019).
- ⁹Q. Liu, W. Miao, Q. Ye, and C. Li, "Performance assessment of an innovative Gurney flap for straight-bladed vertical axis wind turbine," *Renewable Energy* **185**, 1124 (2022).
- ¹⁰A. Bianchini, F. Balduzzi, D. Di Rosa, and G. Ferrara, "On the use of Gurney Flaps for the aerodynamic performance augmentation of Darrieus wind turbines," *Energy Convers. Manage.* **184**, 402 (2019).
- ¹¹T. P. Syawitri, Y. Yao, J. Yao, and B. Chandra, "Geometry optimisation of vertical axis wind turbine with Gurney flap for performance enhancement at low,

- medium and high ranges of tip speed ratios," *Sustainable Energy Technol. Assess.* **49**, 101779 (2022).
- ¹²S. A. Bakhumbsh and M. H. Mohamed, "Effect of micro-cylinder as a passive controller on the Darrieus wind turbine performance," *Ocean Eng.* **266**, 113118 (2022).
 - ¹³S. Acarer, "Peak lift-to-drag ratio enhancement of the DU12W262 airfoil by passive flow control and its impact on horizontal and vertical axis wind turbines," *Energy* **201**, 117659 (2020).
 - ¹⁴S. Abbasi and M. A. Daraee, "Improving vertical-axis wind turbine performance through innovative combination of deflector and plasma actuator," *Phys. Fluids* **36**, 045134 (2024).
 - ¹⁵H. Yu, A. Zhang, and J. Zheng, "Dynamic stall control for a vertical-axis wind turbine using plasma actuators," *AIAA J.* **61**, 4839 (2023).
 - ¹⁶D. You and P. Moin, "Active control of flow separation over an airfoil using synthetic jets," *J. Fluids Struct.* **24**, 1349 (2008).
 - ¹⁷E. Salimpour and S. Yazdani, "Improvement of aerodynamic performance of an offshore wind turbine blade by moving surface mechanism," *Ocean Eng.* **195**, 106710 (2020).
 - ¹⁸X. Zhang and X. Sun, "Performance enhancement of an H-Darrieus vertical axis wind turbine via moving surface boundary-layer control," *Energy Sci. Eng.* **11**, 1180 (2023).
 - ¹⁹J. Sun and D. Huang, "Impact of trailing edge jet on the performance of a vertical axis wind turbine," *J. Mech. Sci. Technol.* **37**, 1301 (2023).
 - ²⁰J. Park and H. Choi, "Effects of uniform blowing or suction from a spanwise slot on a turbulent boundary layer flow," *Phys. Fluids* **11**, 3095 (1999).
 - ²¹P.-L. Delafin, F. Deniset, J. A. Astolfi, and F. Hauville, "Performance improvement of a Darrieus tidal turbine with active variable pitch," *Energies* **14**, 667 (2021).
 - ²²Y. Yang, C. Li, W. Zhang, X. Guo, and Q. Yuan, "Investigation on aerodynamics and active flow control of a vertical axis wind turbine with flapped airfoil," *J. Mech. Sci. Technol.* **31**, 1645 (2017).
 - ²³S. A. Moussavi and A. Ghaznavi, "Effect of boundary layer suction on performance of a 2 MW wind turbine," *Energy* **232**, 121072 (2021).
 - ²⁴N. Aldabash, I. D. Azzawi, and A. Al-Samari, "Experimental and numerical analysis for modification of separated boundary layers over NREL's S822 using blowing/suction techniques," *Int. J. Fluid Mech. Res.* **50**(2), 1–16 (2023).
 - ²⁵E. FatahiAn and H. Fatahian, "Simultaneous effect of suction and cavity for controlling flow separation on NACA 0012 airfoil – CFD approach," *Gazi Univ. J. Sci.* **34**, 235 (2021).
 - ²⁶A. Rezaeiha, H. Montazeri, and B. Blocken, "Active flow control for power enhancement of vertical axis wind turbines: Leading-edge slot suction," *Energy* **189**, 116131 (2019).
 - ²⁷M. Ohashi, Y. Morita, S. Hirokawa, K. Fukagata, and N. Tokugawa, "Parametric study toward optimization of blowing and suction locations for improving lift-to-drag ratio on a Clark-Y airfoil," *J. Fluid Sci. Technol.* **15**, JFST0008 (2020).
 - ²⁸A. M. Elsayed, M. A. Khalifa, E. Benini, and M. A. Aziz, "Experimental and numerical investigations of aerodynamic characteristics for wind turbine airfoil using multi-suction jets," *Energy* **275**, 127503 (2023).
 - ²⁹J. Sun and D. Huang, "Numerical investigation of boundary layer suction control positions on airfoils for vertical-axis wind turbine," *J. Mech. Sci. Technol.* **35**, 2903 (2021).
 - ³⁰G. Tescione, D. Ragni, C. He, C. J. Simão Ferreira, and G. J. W. van Bussel, "Near wake flow analysis of a vertical axis wind turbine by stereoscopic particle image velocimetry," *Renewable Energy* **70**, 47 (2014).
 - ³¹L. Kuang, R. Zhang, J. Su, Y. Shao, K. Zhang, Y. Chen, Z. Zhang, Y. Tu, D. Zhou, Z. Han, Y. Bao, and Y. Cao, "Systematic investigation of effect of rotor solidity on vertical-axis wind turbines: Power performance and aerodynamics analysis," *J. Wind Eng. Ind. Aerodyn.* **233**, 105284 (2023).
 - ³²Z. Wang and M. Zhuang, "Leading-edge serrations for performance improvement on a vertical-axis wind turbine at low tip-speed-ratios," *Appl. Energy* **208**, 1184 (2017).
 - ³³L. Kuang, J. Su, Y. Chen, Z. Han, D. Zhou, K. Zhang, Y. Zhao, and Y. Bao, "Wind-capture-accelerate device for performance improvement of vertical-axis wind turbines: External diffuser system," *Energy* **239**, 122196 (2022).
 - ³⁴J. Su, Y. Chen, Z. Han, D. Zhou, Y. Bao, and Y. Zhao, "Investigation of V-shaped blade for the performance improvement of vertical axis wind turbines," *Appl. Energy* **260**, 114326 (2020).
 - ³⁵A. Rezaeiha, I. Kalkman, and B. Blocken, "CFD simulation of a vertical axis wind turbine operating at a moderate tip speed ratio: Guidelines for minimum domain size and azimuthal increment," *Renewable Energy* **107**, 373 (2017).
 - ³⁶A. Gupta, H. A. Abderrahmane, and I. Janajreh, "Flow analysis and sensitivity study of vertical-axis wind turbine under variable pitching," *Appl. Energy* **358**, 122648 (2024).
 - ³⁷M. T. Javaid, U. Sajjad, S. Saddam ul Hassan, S. Nasir, M. U. Shahid, A. Ali, and S. Salamat, "Power enhancement of vertical axis wind turbine using optimum trapped vortex cavity," *Energy* **278**, 127808 (2023).
 - ³⁸B. Hand and A. Cashman, "Conceptual design of a large-scale floating offshore vertical axis wind turbine," *Energy Procedia* **142**, 83–88 (2017).
 - ³⁹H. Zhu, W. Hao, C. Li, and Q. Ding, "Simulation on flow control strategy of synthetic jet in an vertical axis wind turbine," *Aerosp. Sci. Technol.* **77**, 439 (2018).
 - ⁴⁰X. Sun, Y. Xu, and D. Huang, "Numerical simulation and research on improving aerodynamic performance of vertical axis wind turbine by co-flow jet," *J. Renewable Sustainable Energy* **11**, 013303 (2019).
 - ⁴¹D. Velasco, O. López Mejia, and S. Laín, "Numerical simulations of active flow control with synthetic jets in a Darrieus turbine," *Renewable Energy* **113**, 129 (2017).
 - ⁴²F. R. Menter, R. B. Langtry, S. R. Likki, Y. B. Suzen, P. G. Huang, and S. Völker, "A correlation-based transition model using local variables—Part I: Model formulation," *J. Turbomach.* **128**(3), 413 (2006).
 - ⁴³R. B. Langtry, F. R. Menter, S. R. Likki, Y. B. Suzen, P. G. Huang, and S. Völker, "A correlation-based transition model using local variables—Part II: Test cases and industrial applications," *J. Turbomach.* **128**(3), 423 (2006).
 - ⁴⁴F. R. Menter, "Two-equation eddy-viscosity turbulence models for engineering applications," *AIAA J.* **32**, 1598 (1994).
 - ⁴⁵F. R. Menter, M. Kuntz, and R. Langtry, "Ten years of industrial experience with the SST turbulence model," in *Turbulence, heat and mass transfer* (2003).
 - ⁴⁶Q. Liu, W. Miao, M. Bashir, Z. Xu, N. Yu, S. Luo, and C. Li, "Aerodynamic and aeroacoustic performance assessment of a vertical axis wind turbine by synergistic effect of blowing and suction," *Energy Convers. Manage.* **271**, 116289 (2022).
 - ⁴⁷O. Eboibi, B. E. Eboibi, and L. A. M. Danao, "Solidity effects and azimuth angles on flow field aerodynamics and performance of vertical axis wind turbines at low Reynolds number," *Sci. Afr.* **24**, e02215 (2024).
 - ⁴⁸G. Box and K. Wilson, "On the experimental attainment of optimum conditions," *J. R. Stat. Soc. Ser. B* **13**(1), 1–38 (1951).
 - ⁴⁹S. L. C. Ferreira, R. E. Bruns, H. S. Ferreira, G. D. Matos, J. M. David, G. C. Brandão, E. G. P. da Silva, L. A. Portugal, P. S. dos Reis, A. S. Souza, and W. N. L. dos Santos, "Box-Behnken design: An alternative for the optimization of analytical methods," *Anal. Chim. Acta* **597**, 179 (2007).
 - ⁵⁰C. Carrillo, J. Cidrás, E. Díaz-Dorado, and A. Obando-Montano, "An approach to determine the Weibull parameters for wind energy analysis: The case of Galicia (Spain)," *Energies* **7**, 2676 (2014).
 - ⁵¹K. Sunderland, T. Woolmington, J. Blackledge, and M. Conlon, "Small wind turbines in turbulent (urban) environments: A consideration of normal and Weibull distributions for power prediction," *J. Wind Eng. Ind. Aerodyn.* **121**, 70 (2013).
 - ⁵²A. Rezaeiha, H. Montazeri, and B. Blocken, "A framework for preliminary large-scale urban wind energy potential assessment: Roof-mounted wind turbines," *Energy Convers. Manage.* **214**, 112770 (2020).
 - ⁵³K. Yang, X. Deng, Z. Ti, S. Yang, S. Huang, and Y. Wang, "A data-driven layout optimization framework of large-scale wind farms based on machine learning," *Renewable Energy* **218**, 119240 (2023).
 - ⁵⁴H. Sun and H. Yang, "Wind farm layout and hub height optimization with a novel wake model," *Appl. Energy* **348**, 121554 (2023).
 - ⁵⁵H. F. Lam and H. Y. Peng, "Study of wake characteristics of a vertical axis wind turbine by two- and three-dimensional computational fluid dynamics simulations," *Renewable Energy* **90**, 386 (2016).